REPORT DOCUMENTATION PAGE

Form Approved
OMB No. 0704-0188

1. AGENCY USE ONLY (Leave blank)	2. REPORT DATE	3. REPORT TYPE AND DATES COVERED
	August 1995	Final Technical Report

4. TITLE AND SUBTITLE
Passive Vibration Damping Materials: Piezoelectric Ceramic Composites for Vibration Damping Applications

5. FUNDING NUMBERS
Current No.

N00014-92-J-1391

6. AUTHOR(S)
Shoko Yoshikawa, R. Meyer, J. Witham, S. Yar agadda, G. Lesieutre

7. PERFORMING ORGANIZATION NAME(S) AND ADDRESS(ES)
The Pennsylvania State University
Materials Research Laboratory
University Park, PA 16802

8. PERFORMING ORGANIZATION REPORT NUMBER

9. SPONSORING/MONITORING AGENCY NAME(S) AND ADDRESS(ES)
Office of Naval Research, Code 1131M
Ballstone Tower One
800 North Quincy Street
Arlington, VA 22217-5000

10. SPONSORING/MONITORING AGENCY REPORT NUMBER

11. SUPPLEMENTARY NOTES
N/A

12a. DISTRIBUTION AVAILABILITY STATEMENT
Distribution unlimited.

13. ABSTRACT (Maximum 200 words)

The use of passive piezoelectric damping using PZT ceramics has been demonstrated in theory and the number of experiments. The effort was multifaceted. For application of the shunted passive piezoelectric damping of structural composites, piezoelectric ceramic fibers (PZT family) of several tens of micron diameter were produced using sol-gel spinning process. Since these fibers were not strong enough to withstand handling for continuous poling process, slurry extruded PZT MicroRods,(120 μm in diameter and 10 cm long), were used to establish continuous poling method. The preparation of resistively shunted PZT fiber composites was done using above poled PZT MicroRods. Two attempts to create a shunt circuit within the structural composites are summarized. To further understand and help design shunt PZT damping composite, modeling method was also developed throughout the course of the research.

14. SUBJECT TERMS	15. NUMBER OF PAGES
Shunted passive piezoelectric damping, PZT sol-gel fiber. Fiber piling PZT fiber composite.	77
	16. PRICE CODE

17. SECURITY CLASSIFICATION OF REPORT	18. SECURITY CLASSIFICATION OF THIS PAGE	19. SECURITY CLASSIFICATION OF ABSTRACT	20. LIMITATION OF ABSTRACT
Unclassified	Unclassified	Unclassified	UL

"PASSIVE VIBRATION DAMPING MATERIALS: PIEZOELECTRIC CERAMIC COMPOSITES FOR VIBRATION DAMPING APPLICATION"

GRANT NO. N00014-92-J-1391
Final Technical Report
August 1995

TO:

DEPARTMENT OF THE NAVY
OFFICE OF NAVAL RESEARCH

FROM:

Shoko Yoshikawa
Materials Research Laboratory
The Pennsylvania State University

CONTRIBUTORS:

R. Meyer and J. Witham
Materials Research Laboratory

G. Lesieutre and S. Yarlagadda
Aerospace Engineering

TABLE OF CONTENTS

TABLE OF CONTENTS (Cont.)

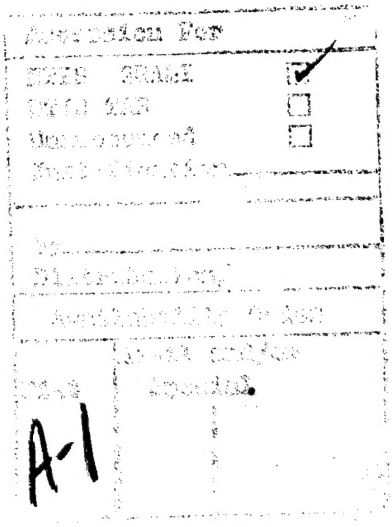

1. INTRODUCTION

This project was initiated originally in January 1990 under ONR's Accelerated Research Initiative "Acoustic Damping Materials" with the purpose of exploring new methods of vibration absorption using a composite system with a ferroic solid as the active phase. The choice of ferroic solid controls the major damping mechanisms, whereas the matrix materials provides mechanical strength as well as stress transfer to the active phase.

Our choice for the active phase is a piezoelectric ceramic material, lead zirconate titanate (PZT). The principle of shunted passive piezoelectric damping was demonstrated using PZT ceramics in both theory and experiment during the first and second years of the contract under Grant No. N00014-90-1540.[1,2] In passive energy dissipation applications, the electrodes of the piezoelectric ceramics are shunted with some electric conductance, hence the term "shunted piezoelectric".

The third year's effort, starting under current contract No. N00014-92-J-1391, was directed at studying the ways in which PZT fibers could be incorporated into structural materials to achieve shunted piezoelectric damping. Fine PZT tubes (1.2 mm in diameter), which are commercially available, were obtained to demonstrate PZT incorporation in structural materials. One of the first methods tried was two-tube PZT modules in a polymer matrix with external resistance. Another approach was to produce PZT tubes in a glass-fiber reinforced epoxy.

One of the most practical methods for large-scale production of structural polymeric materials is to use piezoelectric ceramics in fiber form, which must have high electro-mechanical coupling and must have diameters that are comparable to those of reinforcing fiber materials used in the structural composites. The demonstration of sol-gel derived $PbTiO_3$ and PZT fiber[3,4] indicated that the sol-gel route is the optimum method for producing sub-100 μm diameter piezoelectric ceramic fibers.

The last two years' effort, therefore, was aimed at producing fine PZT fibers by the sol-gel method, at optimizing this sol-gel process, and at establishing methods to pole and to characterize such fine fibers with diameters less than 100 μm. In the meanwhile, demonstration samples for shunted passive piezoelectric damping were planned and prepared using extruded PZT-5H fibers (CeraNova, MicroRods). Detailed experimental procedures and reasons behind designing the sample shape are discussed in this report.

A portion of the effort was also aimed at establishing modeling methods to estimate the achievable damping levels, the shape of frequency-dependence, and the effects of complex stress states and shunting network topology.

2. PZT SOL-GEL FIBER

Due to the limitations on the level of scale-down of the conventional mixed oxide extrusion method, sol-gel or other unconventional ceramic processing is necessary to form several tens of micron diameter fibers.

The PZT fiber formation was demonstrated[4] based on the sol-gel chemistry developed previously for PZT thin films[5]. Later, the prepared solution was transported to Clemson University, Chemical Engineering Department, and fiber was drawn using their spinning apparatus. The detailed information of this process is summarized in Reference 6 (attached).

With the help of the ONR's AASERT (Augmentation Awards for Science and Engineering Research Training) support, a study was conducted to determine the effects of additives and the processing conditions on the sol-gel transition and the fiber drawing ability. The following are a number of variables which are influential on the quality of the solution:

a. Selection of precursors
b. Hydrolysis/humidity
c. pH/acid addition
d. Others

The experiments carried out were: (1) vary the amount of water per mole of PZT starting at 1:1 H_2O:PZT, (2) vary the temperature (room temp., 40, 60, 80°C), and (3) repeat (1) and (2) varying the amount of acid (HNO_3) added during curing starting at 1:1. The detailed information on this portion of research will be summarized in a separate report under ONR Grant # N00014-93-1-1054 shortly.

Under the ARPA contract (Smart Structure Rotor Control Consortium) the fiber spinning apparatus was purchased and the fibers are now drawn in-house. The following composition fibers were prepared and process optimization in progress:

$Pb(Zr_{0.52}Ti_{0.48})O_3$
$PbNb_{0.025}(Zr_{0.53}Ti_{0.47})_{0.976}O_3$
$PbLa_{0.055}(Zr_{0.57}Ti_{0.43})_{0.986}O_3$
$(Ba_{0.5}Sr_{0.5})TiO_3$

Figure 1 shows $Pb(Zr_{0.57}Ti_{0.48})O_3$ fiber spun through 100 micron spinneret orifice followed by pyrolysis and sintering.

The detailed study of electrical and mechanical property of the sol-gel fiber is shown in Reference 6.

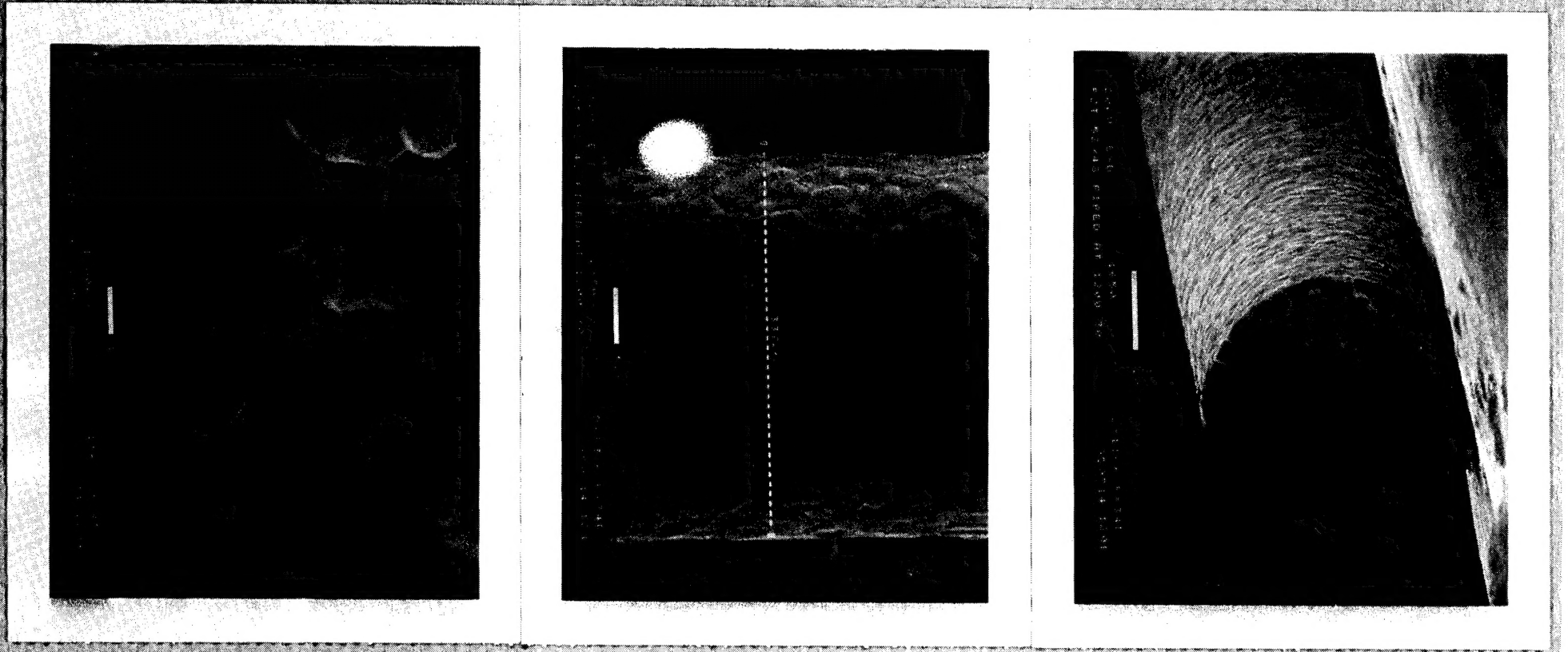

Figure. 1. PZT (52/48) fiber.

In summary, a 30 to 50 μm diameter fiber can be prepared from sol-gel prepared viscous "sol" using spinning apparatus. The drying, pyrolysis, and sintering conditions require careful optimization, which is being conducted currently. Sintering at lower (below lead volatilization of 800°C) temperature gave nearly pure perovskite structure and submicron grain size. All of the following evidence pointed out, however, that the density is low:

— porosity observed by SEM micrograph
— lower dielectric constant
— lower tensile strength

The fibers sintered at temperatures above 1000°C showed apparent densification and grain growth, and show opposite tendencies than those above.

— Lower porosity observed by SEM micrograph
— High (expected) dielectric constant
— Higher tensile strength

Since the inherent strength of PZT family of ceramics is quite low (tensile strength of 50–70 MPa) comparing with that of any structural ceramics, the key of the PZT fiber research lies in the area of the way which produce small grain size with clean (strong) grain boundary but to maintain appropriate piezoelectric properties. The continuous fiber process requires also complete defect-free structure, since any defects will be fiber crack propagation points.

3. PZT MICRO-RODS CONTINUOUS POLING

3.1. Poling Method

Lead zirconate titanate (PZT) ceramics, unlike single-crystal piezoelectric materials such as quartz or Rochelle salt, are polycrystalline materials, which consist of a multitude of tiny, pieozelectric crystallites at random orientation. This random orientation causes the overall ceramic to be inactive, with no piezoelectricity detectable until some means is found to polarize the ceramic as a whole entity. The decisive step here is the poling process: that is, application of a high voltage sufficient to reverse the electric moments of spontaneously polarized regions in the ceramic.

Previous work on poling of fine-scale PZT fibers is limited. Gururaja et al.[7] developed a method for continuous poling of PZT fibers and ribbons with no limit on the length to be poled, but the thickness of the PZT ribbon were limited from 200 to 600 μm for this technique. Under the current contract, a serial poling method for fine-scale PZT fibers was developed[8]; yet, this method had several drawbacks: (a) fine-scale PZT fibers easily broke in the conductive rubber

rings of the sample holder, and (b) only a small section (< 5 mm) of the fiber could be statically poled at one time.

In this investigation, one of the objectives is to continuously pole fine-scale PZT fibers of significant lengths (> 8.0 cm).

Fiber poling study was conducted on 120 μm-diameter PZT-5H fibers (MicroRods) supplied from CeraNova Corporation since they are easier to handle without breaking than sol-gel derived ultra-fine fibers. Figure 2 illustrates apparatus for the fiber continuous poling. A PZT fiber is threaded through two small holes (0.45 mm diameter), one hole in a large stainless steel sphere (10 cm diameter) and the other in a large metal plate (25 cm^2 area), 1 to 2 cm apart. To help thread PZT fiber through these holes, the PZT fiber is attached to the end of a glass rod with a piece of fishing line, and two Teflon grooved rails, one on the far side of the sphere and one of the far side of the aluminum ground plate, are used to keep the glass rod and the PZT fiber aligned with the holes in the sphere and the plate. A metal box with a heater and a fan surrounds this poling apparatus for safety purposes and for heating the air around the apparatus so as to prevent dielectric breakdown. Breakdown field for this apparatus at 60°C is 30 KV/cm, which is the breakdown strength for air.[9] Hence, only PZT fibers of "soft" compositions (i.e., Nb, La-dopants) can be poled continuously in this setup.

With the aluminum plate at ground potential, the sphere is slowly raised to a sufficient voltage so as to exceed the coercive field of the PZT-5H fiber. The reason that the shape for the high voltage side is a sphere is to reduce the breakdown and the corona effects that occur at the sharp edge of the aluminum plate. While the voltage is applied, a PZT-5H fiber is continuously poled as it is being drawn through between the sphere and the plate by pulling the glass rod that is attached to the PZT fiber out of the other end of the metal sphere.

Each one of the 130 fibers, 40 cm long, were poled continuously at 15.0 KV/cm at 55°C. Since the fiber was pulled by hand, it was difficult to determine the speed of fiber motion. The estimated speed is in a range of 1.5–4.5 mm/sec.

3.2. Dielectric and Polarization Measurement

The dielectric properties at room temperature of the PZT-5H fibers were calculated from capacitance measurements using a Hewlett Packard Model 4274 LCR meter and a sample holder shown in Figure 3. An external amplifying circuit was used to boost the sensitivity of the LCR meter by a factor of 100 by increasing the applied signal up to 150 V_{rms}. Poled PZT-5H fibers were cut to 1 and 2 cm-lengths, and a small amount of air-dry silver is applied to both ends of the fibers to ensure electrical contact. Typical dielectric constant values of poled PZT fibers have been previously reported in literature or report.[6,10]

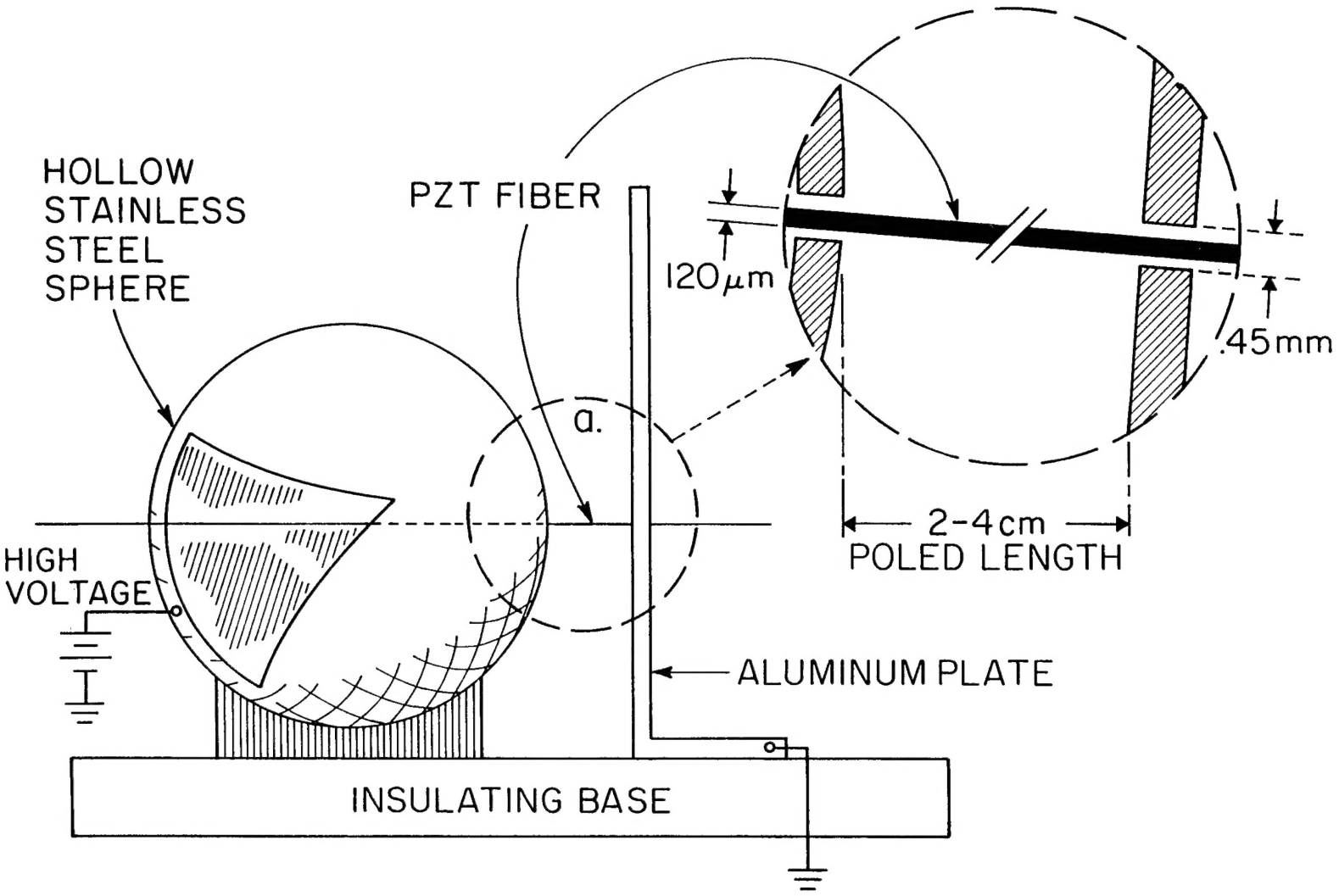

Figure 2. **Fiber poling apparatus. PZT-5H MicroRods are poled at fields of 15.0–17.5 KV/cm for 30–60 seconds. Fibers can be poled in either a static mode or a continuous mode.**

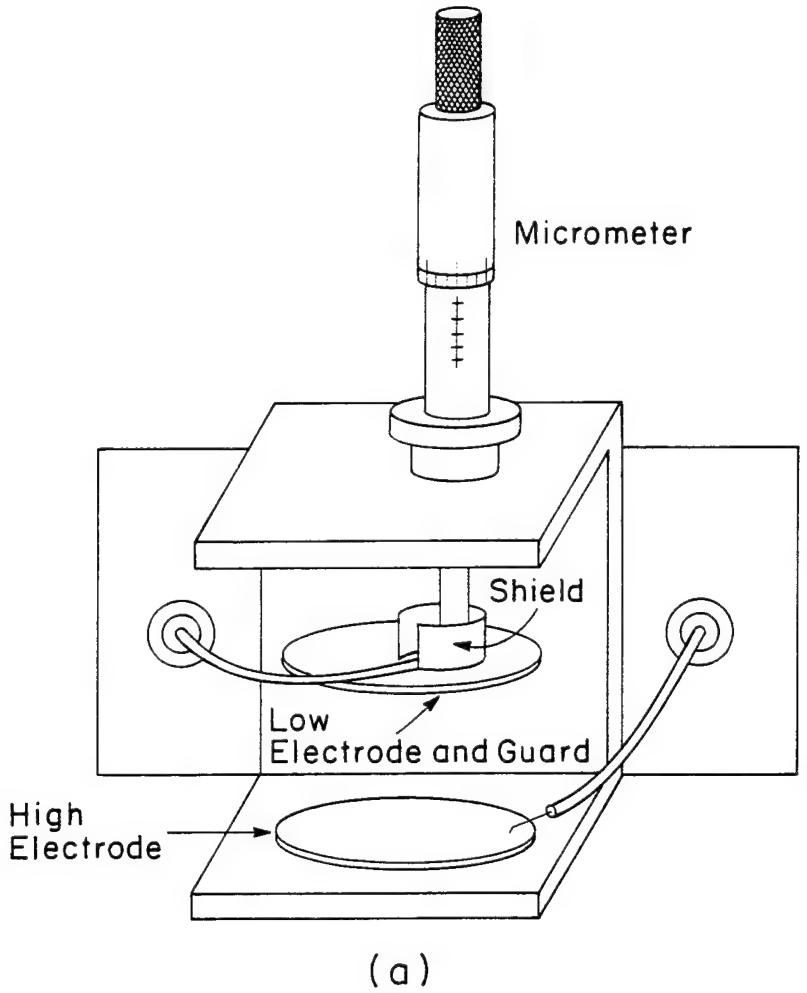

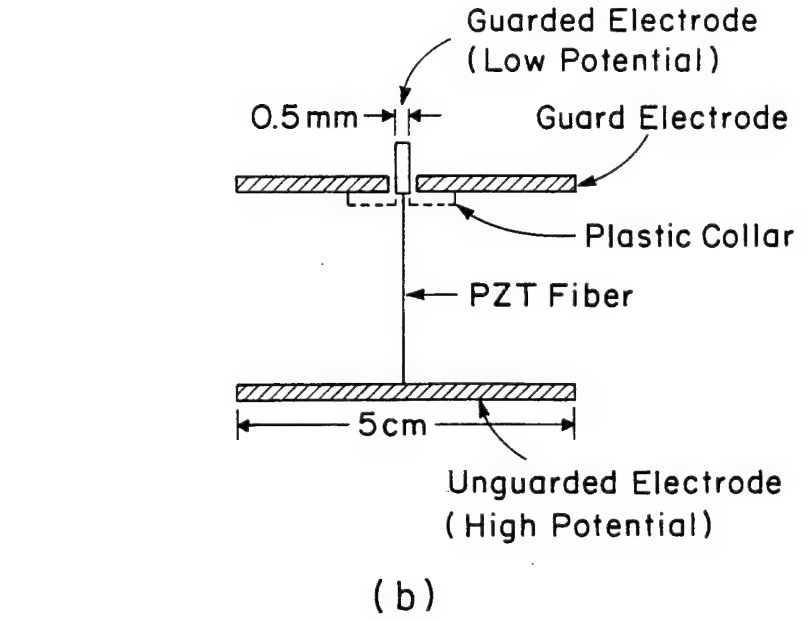

Figure 3. Sample fixture for fiber permittivity and polarization measurement.

The ferroelectric nature of poled PZT-5H fibers was determined through polarization vs. electric field (P-E) measurements using the same sample holder as in the capacitance measurements. Length of poled PZT-5H fibers had to be limited to 3 to 4 mm for testing due to the voltage limitation of the Trek Model 610A High Voltage Power Supply (i.e., 10 KV). A specially designed automated system, shown in Figure 4, was used for this measurement, which applied the field and collected the charge from a poled PZT fiber while maintaining a ground state, similar to a Sawyer-Tower measurement, but the charge was collected by active circuitry rather than a passive capacitor. Fields of > 30 KV/cm at a frequency of 10 Hz are used in the polarization measurement. To avoid breakdown, the sample holder was immersed in a fluorocarbon liquid.

One of the methods for determining if the MicroRods were poled or not involved the polarization setup. The polarization setup is primarily used to show the ferroelectric nature of the PZT ceramic fibers (e.g., remanent polarization (P_R) and coercive field (E_c)), but it also could be used to show if a fiber is poled or not by measuring the polarization of the very first loop (Figure 5A (unpoled) vs. Figure 5B (poled)). Also, with the polarization setup, it is possible to determine which direction the fiber is poled (Figure 5B vs. Figure 5C). Nevertheless, the degree of poling for PZT fibers is difficult to determine by this method.

Other methods for measuring the degree of poling (or polarization) for the PZT fibers that have not been attempted in this investigation to time constraints but should be included for future research are: (a) thermal depoling, (b) photoresponse probe, and (c) optical dilatometry. In the thermal depoling method, polarization of the poled PZT fiber is determined by measuring the charge from the fiber as it is being heated through the Curie temperature. Thakoor and Maserijan found a photoresponse probe of the space charge distribution in ferroelectric PZT thin film memory capacitors to be a good qualitative measurement of the space charge ferroelectric films. It might be possible to apply this technique to measure the charge form poled PZT fibers. Optical dilatometry would be similar to the optical microprobe technique, except a laser interferometer would be used to measure the change in length of the poled fiber (instead of a fotonic sensor).

The reasons why the PZT fibers can be continuously poled are due to the poling apparatus and the geometry of the fibers. With the poling apparatus, the electric field in and around the fiber is almost uniform. The only perturbations in the field are caused by the small holes in the ground plate and the spherical geometry of the high voltage side, but these holes do not significantly affect the field since they are quite small compared to the separation distance and the diameters of the plate and the sphere. As the fiber is being drawn through the holes in the sphere and the plate, the PZT fiber is forced to experience the field between the sphere and the plate, which aligns the domains of the PZT fiber in the longitudinal direction (i.e., in the direction of the electric field). With this continuous poling method, there is no limitation on the length of the PZT fiber that can be poled.

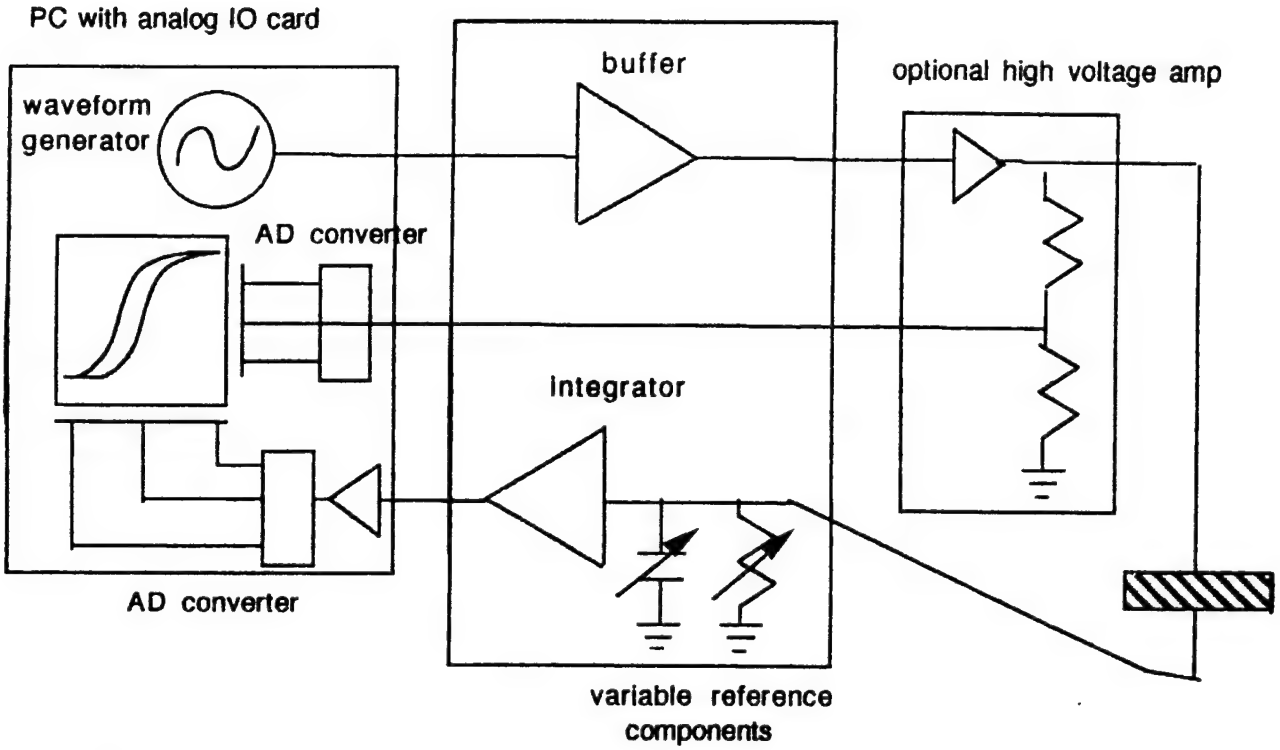

Figure 4. Polarization-Electric Field (P-E) Measurments Setup.

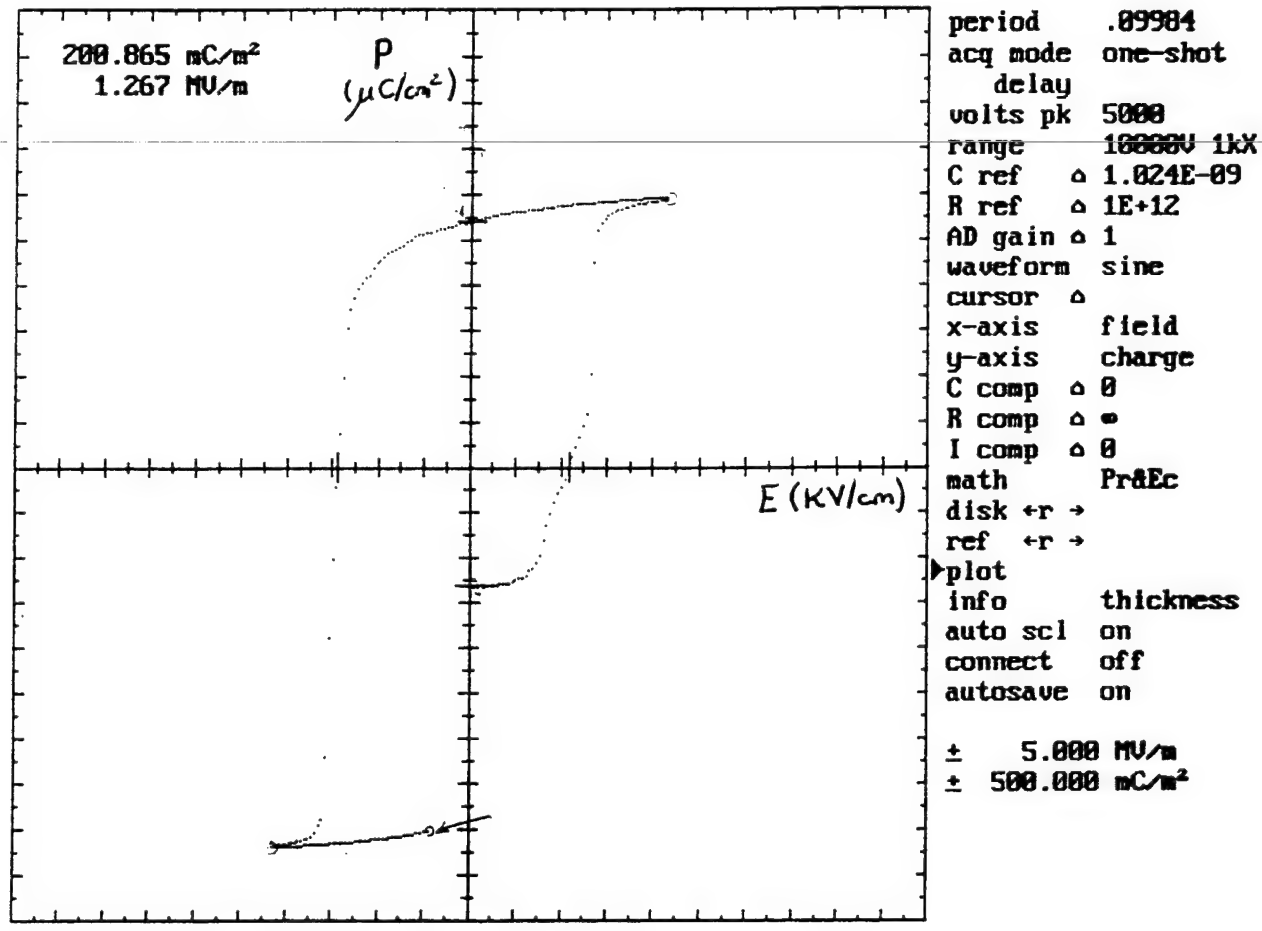

Figure 5A. Hysteresis loop of unpoled CeraNova PZT-5H fiber. Scale for polarization axis is 50 μC/cm2, and the scale for the field (E) axis is 50 KV/cm.

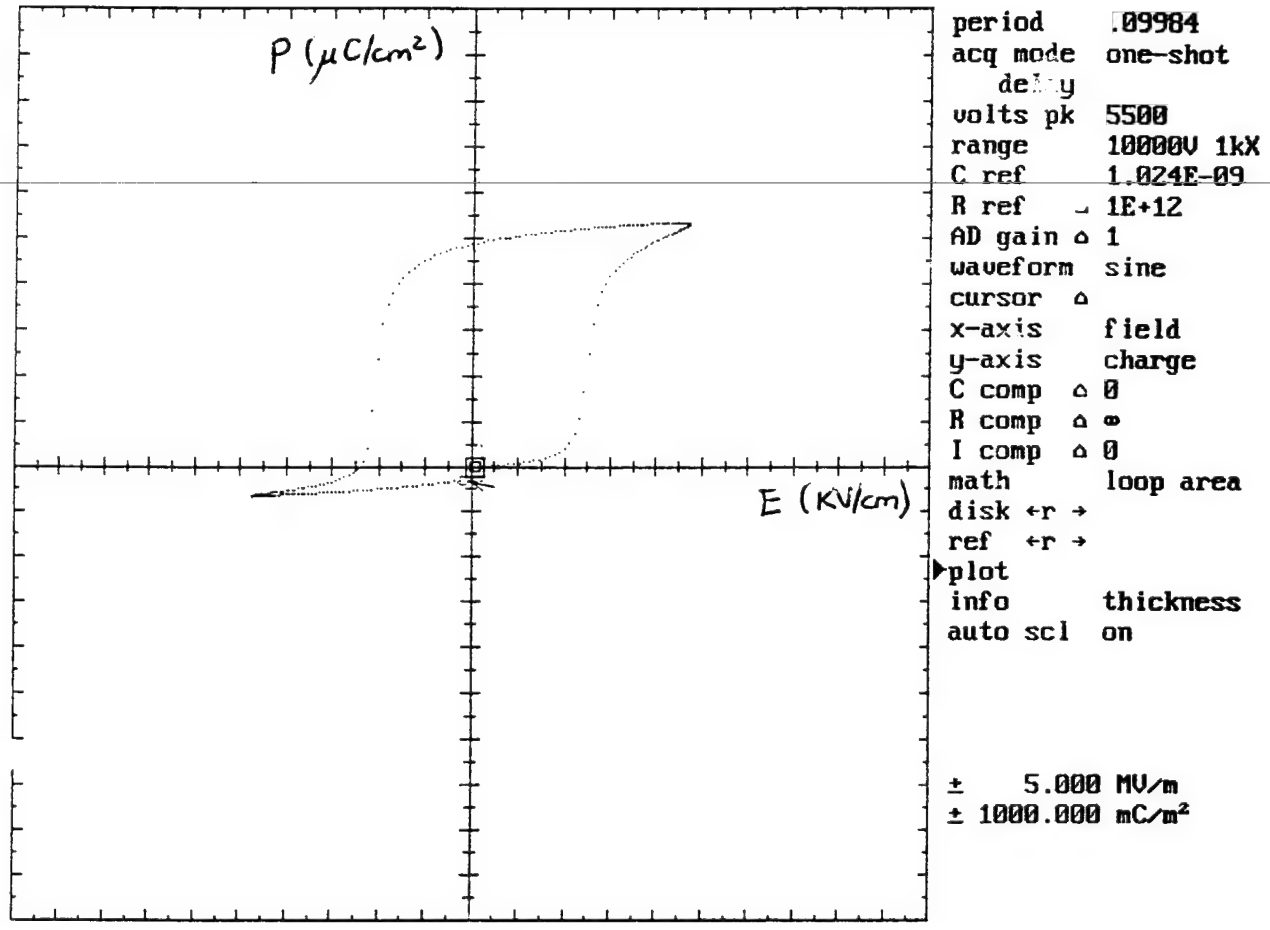

Figure 5B. Hysteresis loop for a poled PZT-5H fiber. Same scales as Figure 8A.

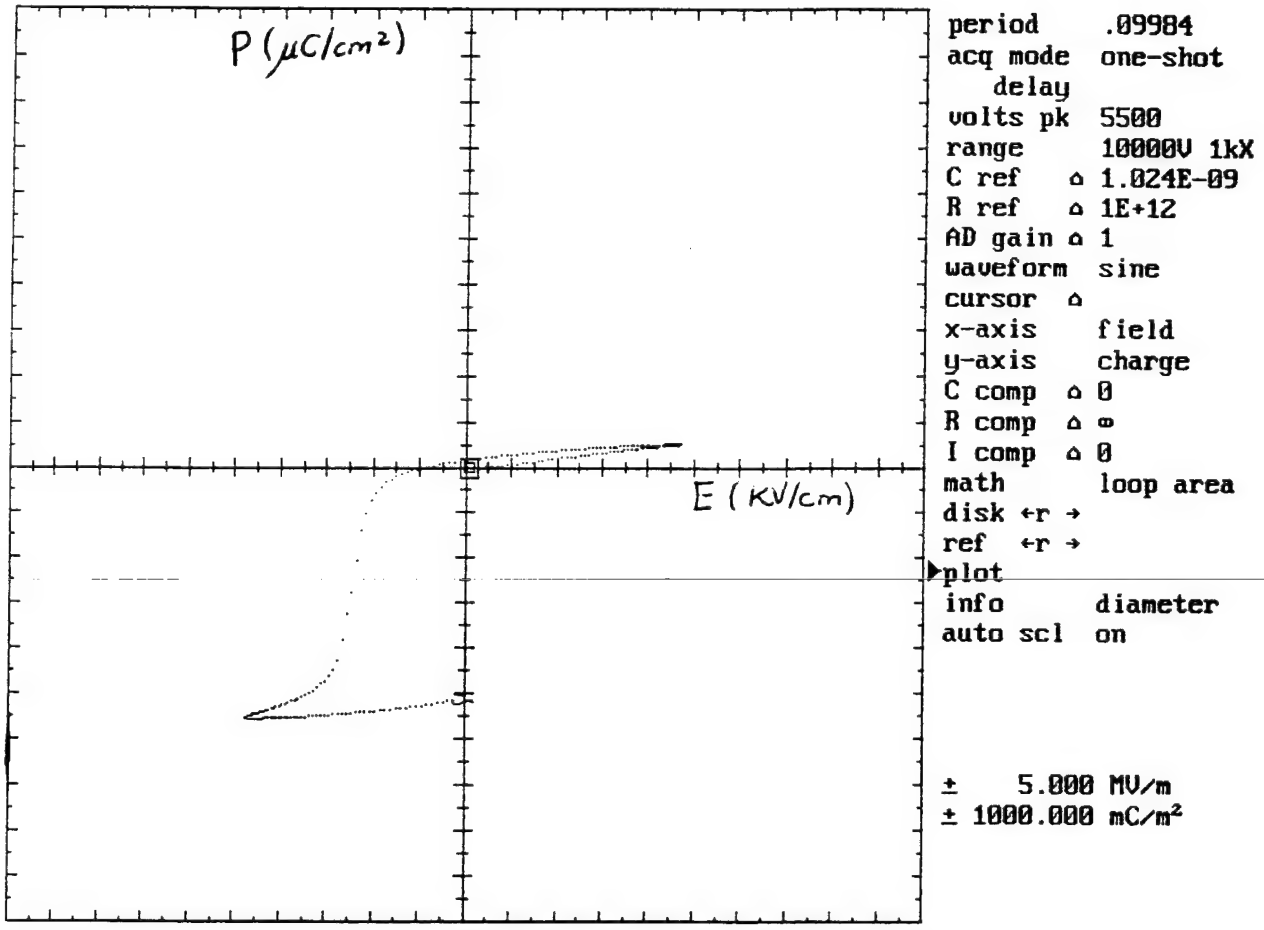

Figure 5C. Hysteresis loop for a PZT fiber poled in the direction opposite to the one for the fiber in Figure 8B. Same scales as Figure 8A.

As the field in the PZT fiber approaches the coercive field (E_C) during poling, charge begins to accumulate in a ring where the fiber is threaded. If the charge is not drawn off, the applied field will be canceled by this accumulated charge. There are several possible mechanisms in which this accumulated charge is dissipated:

1. Corona formation from the surface of the PZT fiber to the circumference of the holes where the fiber is threaded.
2. Air breakdown in the same way a corona is formed.
3. Conduction through the PZT fiber if it is physically touching the circumference of the holes.
4. Surface conduction along the PZT fiber, which is driven by the high field case of 3.

Further experimentation is needed to determine which one of these mechanisms or combination of mechanisms is responsible for dissipation of the accumulated charge. This poling method should exhibit limitations of the PZT diameter, since the poling mechanism relies on the extreme aspect ratio of the PZT between electrode. Breakdown occurred in the poling apparatus when attempts were made to pole PZT fibers with diameters > 200 μm. Diameters larger than 200 μm for PZT fibers cause perturbations in the uniformity of the electric field around the fiber for this particular poling setup, leading to breakdown.

3.3. d_{33} Measurement

Piezoelectric strain coefficient, d_{33}, measurements of PZT-5H MicroRods were made on an optical microprobe setup consisting of: (a) MTI 2000 Fotonic Sensor and (b) Stamford Research Systems SR850 Lock-In amplifier and (c) a sample holder. A few millimeters of MicroRod is mounted perpendicular to the aluminum foil in the sample holder, and electrical contact is made to the PZT rod, the aluminum foil, and the brass block with very small amounts of air-dry silver (Figure 6). A small voltage (5 V_{rms}) is applied to the PZT rod, and the d_{33} value (m/V) is calculated from the amount of deflection experienced by the fiber (as seen by the optical microprobe) divided by the applied voltage. The results of both statically and continuously poled PZT-5H MicroRods are summarized in Table I.

Although possible sources of noise and vibration from the measuring equipment were eliminated from the optical microprobe setup, the measured d_{33} values still showed a variation > ± 20%. The variations in the measured d_{33} values are probably due to the sample holders and how the poled PZT fibers are mounted in them. The aluminum foil in this sample holder could be clamping the poled PZT fibers, which would not allow the poled fiber to deflect when a voltage is applied. The angle and scattering of the light reflection caused by the aluminum foil also created

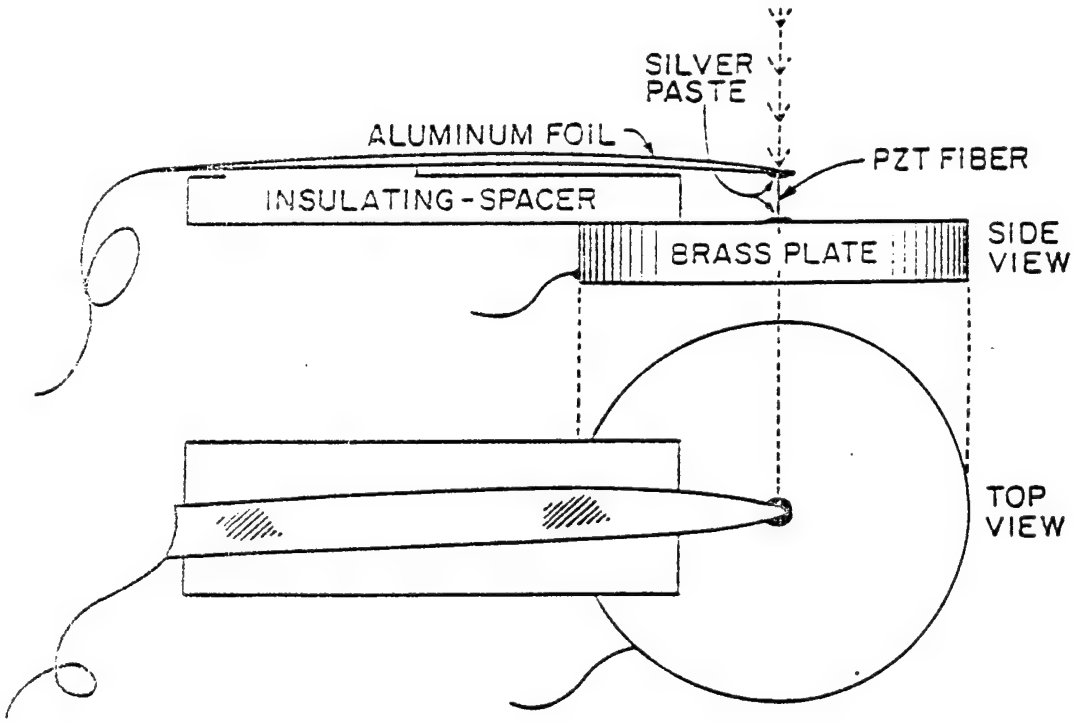

Figure 6. Sample holder for either the optical microprobe or the laser interferometer.

measurement difficulty. The sample holder should be redesigned so that variations in the measured d_{33} values can be eliminated.

Table I. d_{33} Measurements by Optical Microprobe

Poling Method	Poling Field (KV/cm)	Poling Temp. (°C)	d_{33} (10^{-12} m/V)
Static	15.0	57	250–350
Continuous	5.0	57	330–560

Notes: d_{33} value for PZT-5H Bulk Ceramic = $593 \cdot 10^{-12}$ m/V

4. SHUNTED PZT COMPOSITE CONCEPTS

Two types of piezocomposites were considered: continuous fiber and whisker reinforced composites. In both cases PZT-5H fibers of 120 μm diameter were used, as that was the smallest diameter available commercially in bulk quantities. For the whisker reinforced composites, a whisker aspect ratio of 100 was used. Two shunting techniques were examined: resistive coating of piezoelectric fibers and conductive matrix. A fifth piezocomposite configuration, consisting of piezoelectric fibers in a layer of epoxy and shunted by a thin film resistor, was also considered. The following sections describe each of the above cases and discuss the advantages/disadvantages involved.

4.1. Continuous Fiber Piezocomposites

The initial focus in the development of piezocomposites was on continuous fiber piezocomposites with a resistive coating. Continuous fibers were chosen as a first step because of manufacturing issues. The initial plan was to develop an "assembly-line" setup to draw the ceramic fibers, pole the fibers, coat the fibers with a resistive material and embed them in a layer of epoxy to form prepregs. Modeling issues are discussed in the following sections.

4.1.1. Analytical Model

The matrix was assumed to be isotropic and elastic and the fiber was assumed to be transversely isotropic. Perfect bonding was assumed between the fiber, coating and matrix. The entire structural domain was treated as a piezoelectric medium, with the matrix and coating

assumed to have zero piezoelectric properties. A typical representative volume element (RVE) is shown below.

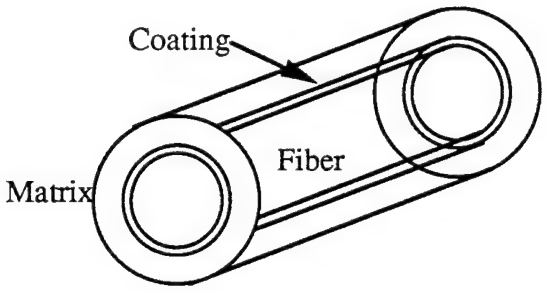

Figure 7. Representative Volume Element

The resistive coating on the piezoelectric fiber is treated as an electrical boundary between the fiber and the matrix. The volume fraction of the resistive coating is much smaller than that of the fiber or the matrix and the coating is assumed to play no other role than dissipating electrical energy developed in the piezoelectric fiber. The quasi-static assumption of the linear piezoelectric theory is valid since the phase velocities of electromagnetic waves are much higher (6 orders of magnitude) than that of waves due to structural vibration.

The resistive coating on the fiber serves as the electrical path for charge developed on the surface of the piezoelectric fiber. Flow of charge within the resistive coating dissipates energy. As the model examines spatial and time-dependent behavior of electric potential and the charge distribution within the piezoelectric fiber, the electric field within the fiber need not be assumed to be uniform.

To describe the electromechanical behavior of the structure, two dependent fields, u (mechanical displacement) and ϕ (electric potential) are defined. Two coupled 3-D differential equations (momentum and charge conservation) governing the spatial and time-dependent behavior of each field were developed:

$$\begin{aligned} C^{E}_{ijkl}\, u_{k,li} + e_{kij}\, \phi_{,ki} &= \rho_o\, \ddot{u}_j \\ \left\{ e_{ikl}\, \dot{u}_{l,k} - \varepsilon_{ik}\, \dot{\phi}_{,k} \right\}_{,k} - \sigma_c\, \phi_{,kk} &= 0 \end{aligned} \qquad (3.1)$$

The boundary conditions for the RVE are as follows:

- At the surface of the fiber, tractions are zero

- The radial stress, $\sigma_r = 0$ everywhere on the surface
- The coating acts as an electrical boundary condition.

Detailed steps in the derivation of Eqns. (3.1) are described in the following chapter.

4.1.2. Resistive coating dynamics

For an applied mechanical loading on the RVE, the resistive coating will conduct/dissipate electrical energy if there are surface charges on the piezoelectric fiber. The surface charge can be expressed in terms of the "local" polarization vector of the piezoelectric fiber. The "local" polarization vector is important because the resistive coating is a continuous conductor/dissipater along the fiber length.

Consider an imaginary surface element dS situated in a polarized dielectric (piezoelectric fiber), as shown in Fig. 8. Let the local polarization vector in the neighborhood of dS be **P**, and the angle between dS and **P** be α. In the process of polarization of the dielectric, the surface dS is crossed by a certain number of positive charges in one direction, and by a certain number of negative charges in the other direction. The total charge that crossed the surface dS in its positive direction in the process of polarization is

$$dQ = \mathbf{P} \cdot d\mathbf{S} \qquad (3.2)$$

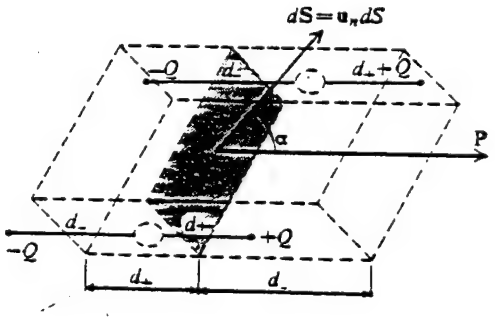

Figure 8. Surface Element Showing Motion of Charges During Polarization of Dielectric

and, for a very small imaginary closed surface ΔS, the total charge that left the volume enclosed by the surface ΔS in the process of polarization is,

$$\Delta Q = \oint_{\Delta S} \mathbf{P} \cdot d\mathbf{S} \tag{3.3}$$

The volume density of charge remaining in the closed area is -ΔQ and the charge density for a very small ΔS is given by

$$\rho_p = -\frac{\Delta Q}{\Delta v} = -\nabla \cdot \mathbf{P} \quad \text{(volume density of bound charges)} \tag{3.4}$$

The density ρ_p is not the density of the free charges, but the mean density of charges bound to their respective atoms. The charges result from the fact that in the process of polarization the balance on positive and negative charges in a physically small volume might be disturbed. Charges thus created in a polarized dielectric are called polarization charges.

Consider now the boundary surface of a dielectric and a vacuum. Assume that the local polarization vector P of the polarized dielectric near the surface makes an angle a with the unit vector $\mathbf{u_n}$ normal to the surface, as shown in Fig. 9. Uncompensated polarization charges exist in the thin layer indicated in the figure. The thickness of this layer is extremely thin and the charges can be assumed to be distributed over the surface of the dielectric. The surface density of the polarization charges is

$$\rho_{sp} = P\cos(\alpha) = \mathbf{P} \cdot \mathbf{u}_n$$

If the local polarization vector P is normal to the unit vector of the surface dS, the surface charge density is zero. For the case of an axially polarized piezoelectric fiber, if the polarization vector is axial everywhere in the fiber, the charge developed on the surface of the fiber is zero, because the surface unit vector is radial and normal to the axial polarization vector. The charge is developed at the ends of the fiber.

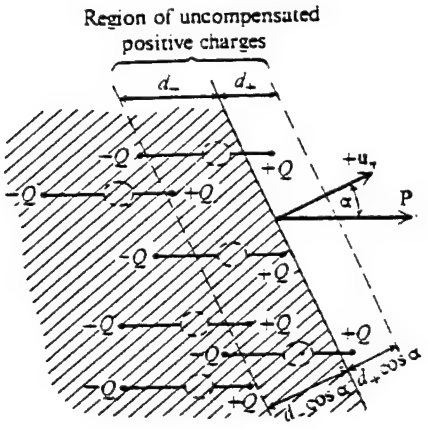

Figure 9. Boundary Surface Between a Dielectric and a Vacuum

Thus, the effectiveness of the continuous resistive coating as a shunting technique for continuous PZT fiber composites depends on the polarization vector of the fiber.

4.1.4. Fiber Poling Direction

The method described in Chapter 3.1 has been successful in poling continuous fibers. However, it is clear from the poling setup and the method, that the polarization vector is not axial at all points within the fiber. Since the dipoles within the PZT fiber orient along the applied field lines, the dipole orientation at points where the fiber is threaded through the holes, is not axial. The speed with which the fiber is moved axially also determines the direction of the local polarization vector.

If the local polarization vector is not axial everywhere in the fiber, there will be charge developed on the surface of the fiber and the resistive coating will be effective in energy dissipation. Modeling the effect of a non-axial polarization vector in a PZT fiber is a very complex task and not the focus of this work. The problem is even more complicated, if the conductive matrix is used as the shunting technique. If surface charges are developed on the fiber, many different resistive paths for flow of charge in a conductive matrix are possible, compared to the single resistive path in the resistive coating case. Modeling multiple resistive paths is out of the scope of this work.

Hagood *et al.*[11] have used a different technique for the manufacture of continuous fiber piezocomposites. Mono-fiber layer specimens were manufactured by hand-layup of unpoled PZT-

5H fibers in epoxy. The layer was electroded using interdigitated electrodes on the top and bottom surface of the piezocomposite ply. By applying an electric field to the electrodes, the fibers were poled in segments, along the length. The resulting polarization vector was axial at most points in the fiber and radial outward at the electrodes. The inhomogenity of the field depended on the electrode spacing and the electrode width to the ply thickness. This technique may provide one possible way to use continuous fibers for passive damping, even though the polarization vector is locally varying, by effectively "segmenting" the fibers.

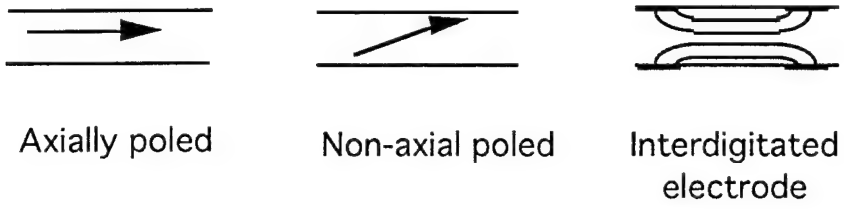

Figure 10. Schematic of Continuous Fiber Poling Directions

If the fiber is axially poled, the resistive coating still acts as a shunt resistor between the two ends of the fiber. However, in that case the continuous fiber is not a good choice because the length of fiber is a critical parameter. Consider the case of a sinusoidal strain distribution. If the fiber length is of the same order as the wavelength, no voltage appears across the ends of the fiber and no damping can result. Thus, the fiber length must be smaller than the wavelength of the mode in consideration, for non-zero damping. Note, that this is independent of the resistive shunting technique used.

Discontinuous PZT fibers(whiskers) offer a way to circumvent this problem. For these fibers, the polarization vector can be assumed to be effectively axial (in the 3 direction) over the fiber length. Hence, the focus of this work changed to short fiber piezocomposites.

4.2. Whisker Piezocomposites

Using short fibers (PZT whiskers) can circumvent the problem of a non-axial polarization vector. The whiskers are assumed to be small enough to exhibit axial polarization throughout the fiber segment. Typical RVEs for a short fiber composite, for both shunting techniques, are shown in Fig. 11.

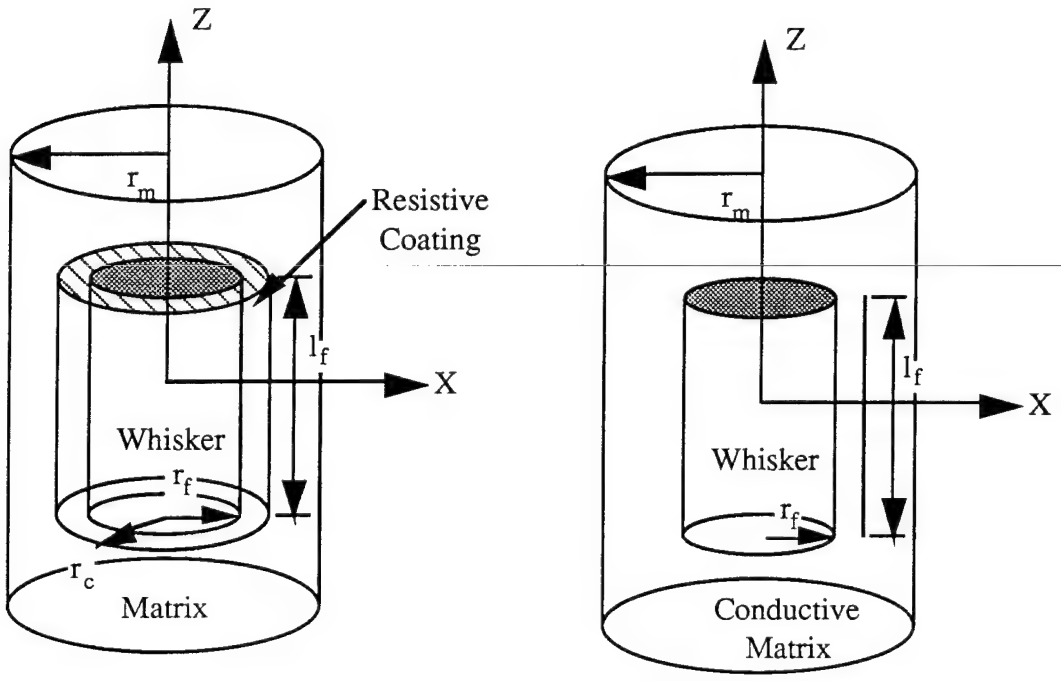

Figure 11. Representative Volume Elements for a Whisker Piezocomposite

The practical advantage to using whiskers instead of continuous PZT fibers is that the brittleness of the fibers and fiber breakage is no longer as significant a problem. From a modeling point of view, the short fiber case is slightly more complicated, because of the stress concentrations at the fiber ends[12]. Generally speaking, smaller fiber lengths are better because the fiber length is then smaller than the wavelength and is no longer a significant factor. However, smaller fiber lengths will also increase the stress concentration effects. As a compromise, an aspect ratio of 100 (1.2cm long segments) was used.

As mentioned earlier, there are two possible shunting configurations: resistive coating each fiber and using a conductive matrix. The following two sections examine each relative merits of each configuration.

4.2.1. Whisker/Resistive Coating Piezocomposite

In the resistive coating case, the whisker is electroded at the ends and the resistive coating serves as a "resistor" between the ends of the fiber segment, as shown in Fig. 11.

Modeling issues

From a modeling point of view, coating the fiber is the simpler of the two. Consider several coated whiskers in a matrix, as shown in Fig. 12. There is only one resistive path for the

flow of charge, from one end of each fiber to the other end of the same fiber. Treating the PZT fiber as a capacitor and the coating as a resistor, the coated fiber represents a parallel RC circuit (Fig. 12) and has a characteristic RC time constant or frequency. The voltage source represents the charge developed across the ends of the fiber due to structural vibration and electromechanical coupling. The frequency of the generated voltage is the structural vibration frequency. Damping is maximum, when the structural frequency matches the characteristic frequency of the circuit. Presence of more than one fiber does not alter the characteristic frequency as each fiber is independent of the other (matrix is an insulator). The number of fibers in the composite determines the volume fraction contribution to modal damping.

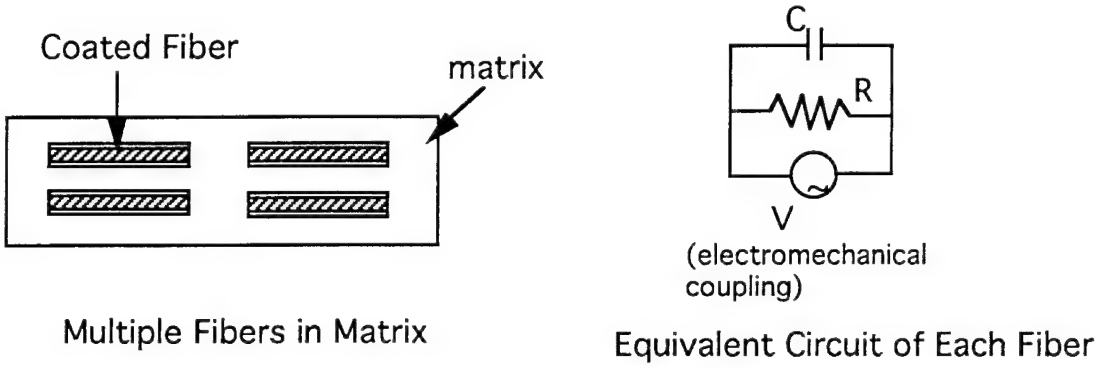

Figure 12. Equivalent Circuit in Resistive Coating Case

Governing equations for this configuration are derived in the detail in the next chapter. The thickness of the resistive coating is a design factor which can be varied to match different resonant frequencies of the structure. An advantage of this shunting technique is the possibility of using different coating thicknesses in the same structure. In this way, damping can be increased at more than one resonant frequency of the structure.

Manufacturing issues

The main drawback to using this shunting technique is the lack of a technique to coat a large number of fibers in a relatively short period of time. Available resistive coating techniques such as sputter deposition, vapor deposition etc. can be used to coat a few fibers at a time. However, since the number of fiber segments needed to obtain a reasonable fiber volume fraction (> 0.10) in a structure is quite high, these techniques cannot produce coated fibers within a short period of time.

Another factor is the temperature during the coating process. Since the fibers are poled, the temperature during the coating process cannot be very high (< 100 °C for PZT-5H) or the fibers will get depoled. Poling after providing a resistive coating to the fibers is not possible, as the coating will provide an alternate path for the flow of charge due to the applied poling field.

4.2.2. Whisker/Conductive Matrix Piezocomposites

An alternative to coating the fibers is to use a conductive matrix to shunt the PZT fibers. Making a conductive matrix is much easier and can be done by adding a conductive filler to an epoxy matrix. Literature[13-15] is available on the resistive properties of a wide range of filler based conductive epoxies.

Modeling issues

However, in the case of the fiber in a conductive matrix, there are a large number of possible resistive paths from one end of the fiber to the other. Flow of charge can occur along any of these paths. Statistically, one can speak of an "average" or "mean" resistive path, which would indicate the effective resistance R and coupled with the capacitance C of the fiber, it determines the characteristic time constant of the system. In the case where there is more than one fiber (as is the case), the problem is even more complicated. There is now the possibility of a resistive path from one fiber to another. There is no simple equivalent circuit as in the case of resistive coating, as summarized in Fig. 13. The effective resistance is now determined by the internal geometry (fiber length, fiber spacing along all three axes) and strain levels in each fiber. An additional feature is the matrix dielectric constant. Addition of a filler to the matrix may increase the dielectric constant of the matrix. Even if it doesn't, the matrix has a capacitance based on its dielectric constant and

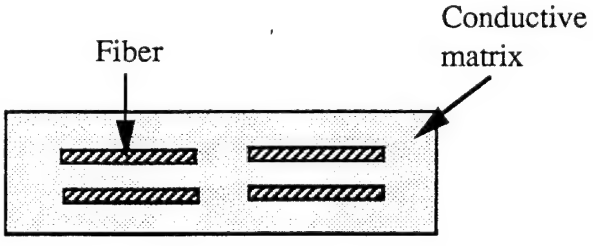

Multiple Fibers in Matrix

Equivalent Circuits:

Fiber (C) - Matrix (R)
R - end to end (same fiber)
R - end to end (diff. fiber)

Matrix (C) - Matrix(R)

Figure 13. Equivalent Circuit in Conductive Matrix Case

combined with its resistance forms another RC type circuit. Thus, using a conductive matrix effectively increases the number internal time constants within the layer. Modeling this type of shunting is more difficult than the case of resistive coating.

Another interesting modeling issue is that the RVE shown in Fig. 11 is no longer valid. This is because of the possible charge flow from one fiber to the adjacent fiber, which means there is charge flow from one RVE to another. Thus, the RVE is no longer a "representative" element in describing the behavior of the system.

Manufacturing issues

The resistivity of the conductive matrix can be explained using the percolation effect[13,14]. The main drawback of the percolation effect, is that there is a large change in resistivity of the matrix over a small filler volume fraction. To control the resistivity of the matrix, it is necessary to be able to control filler volume fraction very accurately (~0.01%) during manufacture. A possible side effect to adding a filler is the change in matrix properties. The changes in matrix mechanical and electrical properties due to the percolation effect has not been well documented. These issues are examined in detail in a later chapter.

4.3. Whisker Piezocomposite with Thin Film Resistor

In this shunted piezocomposite configuration, the whiskers are shunted by a thin film "external" resistor. The whiskers are embedded in a layer of epoxy and cured. The ends of the resulting piezocomposite are electroded and a thin resistive film is deposited on one surface of the piezocomposite. This configuration is a combination of the resistive coating and conductive matrix cases. Instead of shunting a single fiber with a coating, the thin film provides a resistive path from end to end of a group of fibers. An RVE based analysis of this configuration is no longer possible.

4.3.1. Modeling issues

Figure 14 shows a schematic of a thin film shunted piezocomposite. There is only one resistive path for the flow of charge, from one electroded end to the other . The PZT whiskers in the matrix can be treated as a capacitor, based on the effective dielectric constant of the piezocomposite and the dimensions. The thin film can be treated as a resistor, based on the resistivity of the thin film and its dimensions. The voltage source represents the charge developed across the electrodes due to structural vibration and electromechanical coupling in the whiskers. The frequency of the generated voltage is the structural vibration frequency. Damping is maximum, when the structural frequency matches the characteristic frequency of the circuit. The number of fibers determines the volume fraction contribution to modal damping.

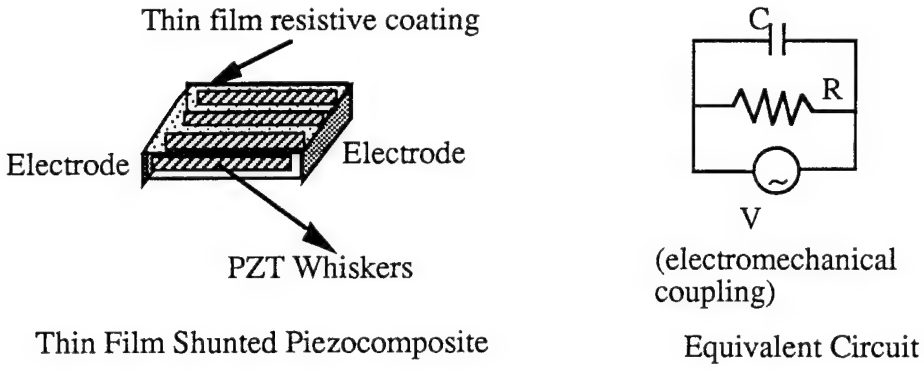

Figure 14. Equivalent Circuit for Thin Film Piezocomposite

A simplified approach to this case, is to consider the PZT whisker/matrix piezocomposite as a piezoelectric material, with effective properties determined by the fiber/matrix properties and the fiber volume fraction. A microelectromechanical model can be used to calculate the effective piezoelectric properties of the composite. The film is treated as a resistor with no influence on the mechanical behavior of the composite. The film thickness is a design parameter and by using different thickness to vary the resistance, different structural modes can be damped.

Manufacturing issues

This configuration has several advantages over the previous two whisker piezocomposite configurations. The fibers need not be poled before manufacture of the piezocomposite. The fibers can be poled after the piezocomposite is cured and electroded by applying the required poling field using a standard poling technique. In this way, high values of d_{33} can be obtained as compared to the continuous poling technique, which is not a standardized technique. Also, the curing time can be reduced by curing at a higher temperature. Manufacture of unpoled piezocomposites is also easier, as there is no need to keep track of the poling direction of each whisker.

The thin films are deposited by a dc-magnetron sputtering of the target in an argon/hydrogen plasma under high vacuum. There is a small temperature increase (~40 °C) of the growing film during deposition due to the bombardment process and the heat of condensation of the evolving film. The thickness of the film can be controlled during deposition by changing the deposition time. This process is described in detail in a later chapter.

4.4. Discussion

Of the five shunted piezocomposite configurations outlined in the preceding sections, each configuration has its advantages and disadvantages. The main criteria for the selection of the "best" configuration for detailed modeling and experimentation are

- ease of manufacture
- ability to model easily and accurately
- availability of poled fibers

Continuous fiber piezocomposites are not a good choice, because the poling direction in the fibers is considered to be axial. Also, the length of the fiber has to be much smaller than the wavelength of the mode being damped.

Of the three whisker piezocomposite configurations, the whisker/conductive matrix and the whisker/thin film piezocomposite were chosen for detailed study and testing for the following reasons:

- Shunting using conductive matrix or the thin film technique is easier from a manufacturing point of view compared to resistive coating each fiber. In order to make a single ply of piezocomposite, a large number of whiskers are required. For example: at 20% PZT volume fraction, to make a 8.5 cm x 1 cm x 200 μm piezocomposite layer, approximately 250 whiskers (1.2 cm long, 120 μm diameter) are needed. Resistive coating of that many fibers in a short period of time is not feasible with current technology and new techniques have to be developed.

- In the thin film case, the fibers can be unpoled during composite manufacture and poled later using a standard poling technique. This solves the problem of limited availability of poled fibers. However, in the conductive matrix case, the fibers have to be poled before composite manufacture.

- While one can develop an electrodynamics model for the resistive coating case using the RVE in Fig. 11, solving the coupled 3-D governing equations is difficult. A different modeling technique is needed for both the thin film and conductive matrix case as the RVE concept is not valid. A simpler micromechanics based finite element model was developed for both these cases and is described in detail in the following chapter.

4.5. Passively Damped Structure Design

In order to demonstrate improved damping, a shunted piezocomposite structure is designed to the specifications of the theoretical model. The model predicts modal frequencies and loss

factors based on the structural parameters and is used to generate optimum structural parameters for maximum loss in a specified mode of vibration.

Since flexural vibration is the easiest to test/measure experimentally, the model will be used to predict modal frequencies and loss factors of the structure in flexural vibration. Another important consideration is the geometry of the piezocomposite layer and the number of available poled PZT fiber segments. Since the poling technique is itself a research topic (for fibers), the number of available poled fibers is limited (~1000 segments of PZT-5H, 1.2 cm long, 120 mm dia.). Based on these facts, the test specimen (Fig. 15) is an aluminum base beam reinforced with a piezocomposite layer.

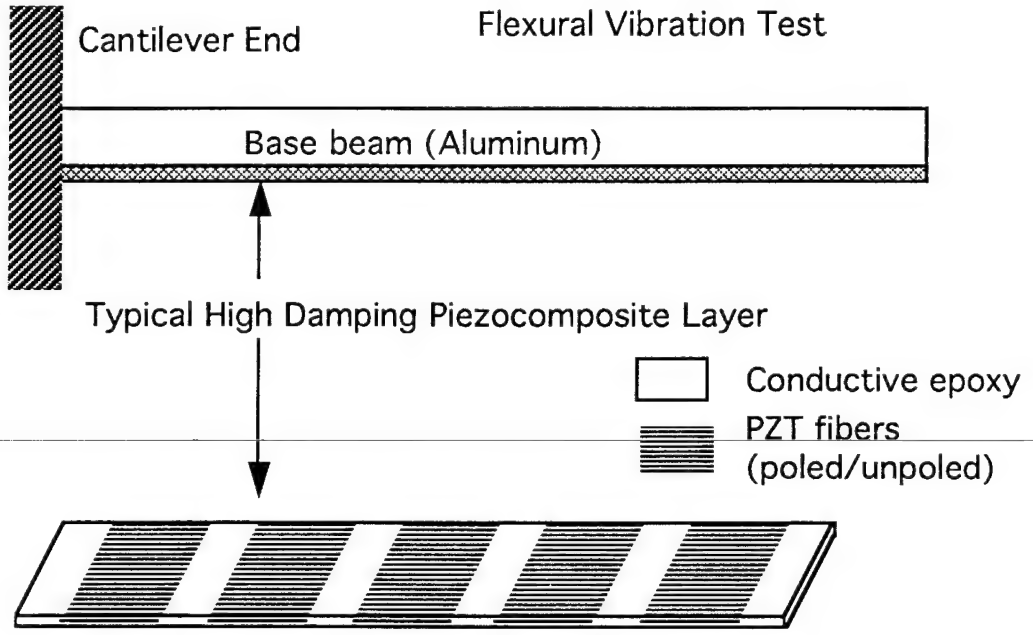

Figure 15. Flexural Test Specimen and Piezocomposite Layer Configuration

The piezocomposite layer is composed of PZT fibers (poled or unpoled) embedded in a conductive matrix. The base beam is aluminum and its cross-section is a design parameter. A rectangular cross-section is the simplest from both modeling and manufacture point of view. However, other cross-sections are also being considered. An I section is a better choice over a rectangular section, because it can retain the bending stiffness while increasing the beam height. The beam height is a design parameter because, in bending, the height of the base beam determines the strain level in the piezocomposite layer. Both sections are being considered for base beam design.

For the whisker/thin film resistor case, a slightly different test specimen will be designed. Figure 16 shows a schematic of the test specimen and setup. The location of each piezocomposite sample on the base beam is a design parameter. Also the length of the piezocomposite sample must be smaller than the wavelength of the mode that is to be damped. The base beam is the same as in the conductive matrix case.

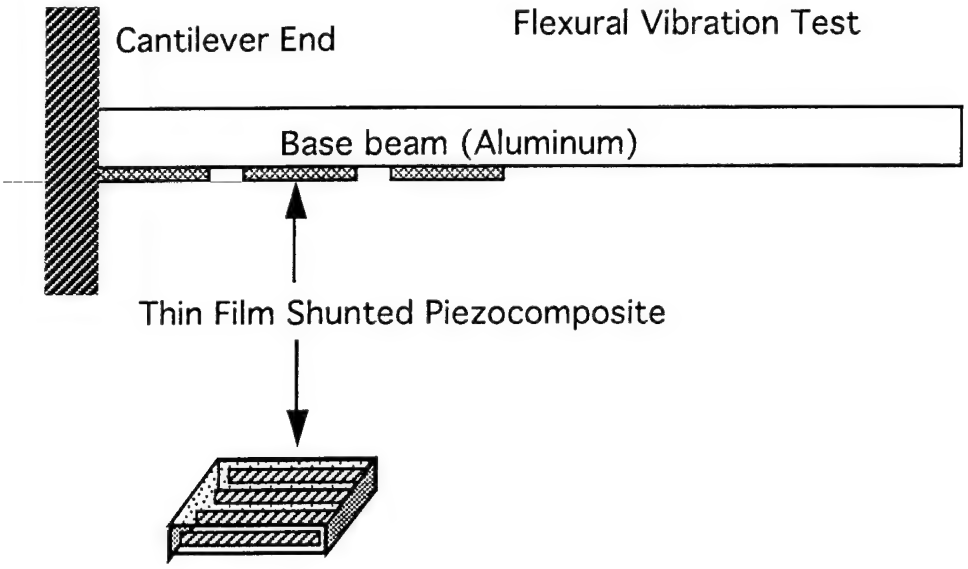

Figure 16. Flexural Test Specimen for Thin Film Piezocomposite Case

For both conductive matrix and thin film cases, predicted increases in damping will be compared to experimentally measured values.

5. PIEZOCOMPOSITE MODELING

Using a simple micromechanics based model[16] it was demonstrated that high damping levels that could be achieved using resistance shunted piezoelectric fibers. Experimental results validating the general concept of shunted piezoelectric damping using monolithic elements have been reported in the literature[17-19]. The next step is to develop a detailed analytical model. The following sections describe analytical and finite element models for whisker piezocomposites.

5.1. Micro-Electromechanics Model

An RVE consisting of a single piezoelectric fiber in a cylinder of conductive matrix was modeled. A schematic of the RVE is shown in Fig. 17. Poling direction of the piezoelectric fiber

is along the fiber length. Equations governing the behavior of the domain are formulated in the following sections.

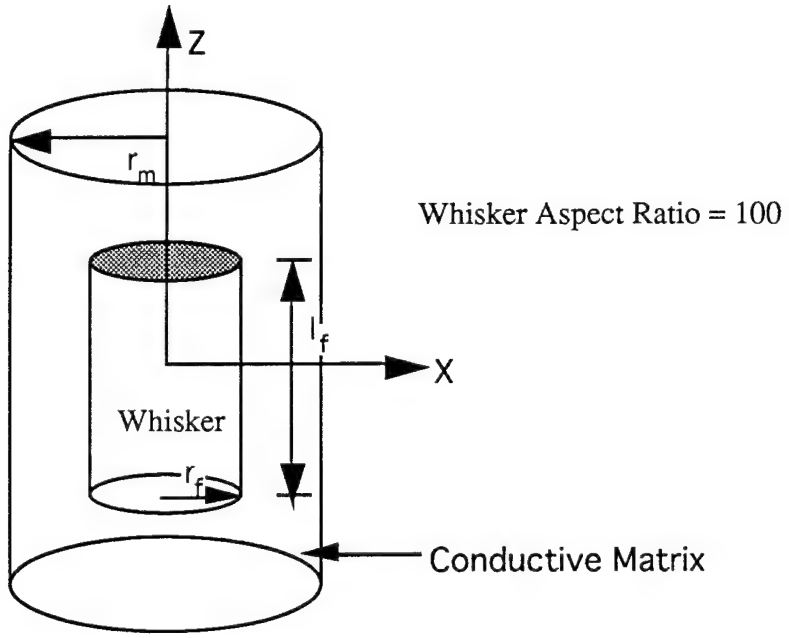

Figure 17. Representative Volume Element for a Whisker Piezocomposite

The idea behind developing an electro-micromechanics model, is to be able to determine the complex mechanical properties (stiffness and damping) of an RVE from that of its constituents by modeling the interactions between the constituent phases in the RVE. After the effective complex mechanical properties of the piezocomposite layer are calculated, we use a structural dynamic model (based on complex moduli) to predict modal frequencies and loss factors.

5.1.1. Formulation

The following assumptions were made:

- The matrix was assumed to be isotropic and elastic and the fiber was assumed to be transversely isotropic. Perfect bonding is assumed between the fiber and matrix. Porosity is assumed to be negligible.
- The matrix is assumed to have zero piezoelectric properties, but a non-zero dielectric constant and conductivity. Conductivity in the piezoelectric fiber is assumed to be zero.

- The volume fraction of the filler in the matrix is a design parameter. The filler particle size (typically 0.5 μm) is assumed to be small compared to fiber dimensions. Effective properties of the conductive matrix are calculated using micromechanical models.
- Quasi-static assumption of the linear piezoelectric theory is valid since the phase velocities of electromagnetic waves are much higher (6 orders of magnitude) than that of waves due to structural vibration. The model is focused on examining the spatial and time-dependent behavior of electric potential and charge distribution within the piezoelectric fiber/resistive coating.
- There were no "electrodes" on the piezoelectric fiber. Instead, the conductive matrix serves as the external electrical path for charge developed in the piezoelectric fiber. Flow of charge within the matrix dissipates energy.
- As the model examines spatial and time-dependent behavior of electric potential and the charge distribution within the piezoelectric fiber, electric field within the fiber was not assumed to be uniform.

To describe the electromechanical behavior of the RVE, two coupled dependent fields, u (mechanical displacement) and ϕ (electric potential) are defined. Two coupled differential equations governing the spatial and time-dependent behavior of each field are developed. Momentum conservation governs the elastic behavior, while charge conservation governs the electrical behavior of the RVE. Separate equations are derived for the matrix and the fiber, with common boundary conditions at the interfaces.

5.1.2. Constitutive Equations

For the piezoelectric fiber, the constitutive equations for the domain (from linear piezoelectric theory) are

$$\begin{aligned} \sigma_{ij} &= C^{E}_{ijkl}\, S_{kl} - e_{kij}\, E_k \\ D_i &= e_{ikl}\, S_{kl} + \varepsilon_{ik}\, E_k \end{aligned} \qquad (5.1)$$

where, σ is stress, S is strain (a function of u), E is the electric field (a function of ϕ), and D is the electric displacement. ε are the dielectric permittivities, e are the piezoelectric constants and C are the material elastic constants at constant field.

5.1.3. Time-Dependent Behavior of u

Momentum conservation for a general domain can be expressed as

$$\sigma_{ij,j} = \rho_o \ddot{u}_j \tag{5.2}$$

where ρ_o is the density of the structure and body forces are zero. Substituting for the stress σ using the constitutive equation in the preceding equation

$$C^E_{ijkl}\, u_{k,li} + e_{kij}\, \phi_{,ki} = \rho_o \ddot{u}_j \tag{5.3}$$

The above equation is a general 3-D differential equation governing the behavior of u and is coupled to ϕ through the piezoelectric constants e_{kij}.

5.1.4. Time-Dependent Behavior of ϕ

To develop charge and potential dynamics, charge conservation and Ampere's Law for a general electromagnetic domain were examined.

$$\begin{aligned} &\frac{\partial q}{\partial t} + \nabla \bullet J = 0 \\ &\oint_{\ell} H \bullet dr = \int_{s} n \bullet \dot{D}\, ds + \int_{s} n \bullet J\, ds \end{aligned} \tag{5.4}$$

q is the charge density, J the current flux, H the magnetic field intensity and D the electric displacement. Integration over *l* and *s* represent line and surface integrals in a plane, respectively. For a non-magnetic domain H is zero. Applying the Divergence theorem to both surface integrals in Ampere's Law,

$$\int_V \nabla \cdot \dot{D}\, dv + \int_V \nabla \cdot J\, dv = 0 \tag{5.5}$$

Differentiating the second constitutive equation with respect to time, and with respect to spatial coordinates

$$\nabla \cdot \dot{D}_i = \left(e_{ikl}\, \dot{u}_{l,k} - \varepsilon_{ik}\, \dot{\phi}_{,k}\right)_{,k} \tag{5.6}$$

where, in the general case, k = 1, 2, 3. The current flux within the domain is restricted to that within the conductive matrix and assuming the fiber to be non-conductive (or very high resistance compared to the resistive coating), the current flux J in the domain is

$$J_k = -\sigma_{c_r}\, \phi_{,k} \tag{5.7}$$

where σ_{c_r} is the electrical conductivity of the conductive matrix. Substituting the above equations in the modified form of Ampere's Law

$$\int_V \left[e_{ikl}\, \dot{u}_{l,k} - \varepsilon_{ik}\, \dot{\phi}_{,k}\right]_{,k} dV + \int_V -\sigma_{c_r} \left[\phi_{,k}\right]_{,k} dV = 0 \tag{5.8}$$

where, in the general case, k = 1, 2, 3. The above equation is a 3-D equation governing the spatial and time-dependent behavior of ϕ coupled to u by the piezoelectric constants.

Eqn. (5.8) is applicable to a general domain that has piezoelectric and conductive properties. Since the fiber is assumed to be non-conductive, the conductive term drops out for the fiber and since the matrix is not piezoelectric, the term involving e drops out.

5.1.5. Governing Equations for RVE

Since the RVE is axi-symmetric, the 3-D equations (5.3 & 5.8) can be reduced to the following form for the piezoelectric fiber:

$$C_{11}^{E}\left[\frac{\partial^2 u_r}{\partial r} + \frac{1}{r}\frac{\partial u_r}{\partial r} - \frac{u_r}{r^2}\right] + C_{44}^{E}\frac{\partial^2 u_r}{\partial z} + (e_{15}+e_{31})\frac{\partial^2 \phi}{\partial r\,\partial z} = \rho_o \frac{\partial^2 u_r}{\partial t^2}$$

$$C_{33}^{E}\frac{\partial^2 u_z}{\partial z^2} + (C_{13}^{E}+C_{44}^{E})\left[\frac{\partial^2 u_r}{\partial r\,\partial z} + \frac{1}{r}\frac{\partial u_r}{\partial z}\right] + e_{33}\frac{\partial^2 \phi}{\partial z^2} + e_{15}\left[\frac{\partial^2 \phi}{\partial r^2} + \frac{1}{r}\frac{\partial \phi}{\partial r}\right] = \rho_o \frac{\partial^2 u_z}{\partial t^2} \qquad (5.9a\text{-}c)$$

$$\frac{\partial}{\partial t}\left\{e_{33}\frac{\partial^2 u_z}{\partial z^2} + (e_{15}+e_{31})\left[\frac{\partial^2 u_r}{\partial r\,\partial z} + \frac{1}{r}\frac{\partial u_r}{\partial z}\right] - \varepsilon_{33}\frac{\partial^2 \phi}{\partial z^2} - \varepsilon_{11}\left[\frac{\partial^2 \phi}{\partial r^2} + \frac{1}{r}\frac{\partial \phi}{\partial r}\right]\right\} = 0$$

where u_r is the radial displacement and u_z is the axial displacement along the fiber. All three degrees of freedom (u_r, u_z and ϕ) are functions of r and z coordinates. They are independent of the theta direction due to symmetry. Note that there no conduction term in the electrical equation (5.9c) as a result of which the electrical equation is effectively electrostatic within the piezoelectric. This is a typical feature in piezoelectric analyses. In this case, however, ϕ will not be static, as there is conduction in the matrix. Eqns 5.9a-c are similar to the governing equations for 1-3 piezocomposites derived in the literature[20-22].

For the conductive matrix:

$$C_{11}\left[\frac{\partial^2 u_r}{\partial r} + \frac{1}{r}\frac{\partial u_r}{\partial r} - \frac{u_r}{r^2}\right] + C_{44}\frac{\partial^2 u_r}{\partial z} = \rho_o \frac{\partial^2 u_r}{\partial t^2}$$

$$C_{33}\frac{\partial^2 u_z}{\partial z^2} + (C_{13}+C_{44})\left[\frac{\partial^2 u_r}{\partial r\,\partial z} + \frac{1}{r}\frac{\partial u_r}{\partial z}\right] = \rho_o \frac{\partial^2 u_z}{\partial t^2} \qquad (5.10a\text{-}c)$$

$$\varepsilon_m \frac{\partial}{\partial t}\left\{\frac{\partial^2 \phi}{\partial z^2} + \left[\frac{\partial^2 \phi}{\partial r^2} + \frac{1}{r}\frac{\partial \phi}{\partial r}\right]\right\} + \sigma_{cm}\left\{\frac{\partial^2 \phi}{\partial z^2} + \left[\frac{\partial^2 \phi}{\partial r^2} + \frac{1}{r}\frac{\partial \phi}{\partial r}\right]\right\} = 0$$

where σ_{cm} is the matrix conductivity and ε_m is the matrix dielectric permittivity. The electrical equation is a first order p.d.e in time.

The boundary conditions relating the two regions (matrix and fiber) are

elastic: $u_i^m = u_i^f$ $\sigma_i^m = \sigma_i^f$ (5.11a)

electric: $\phi_f = \phi_m$ on the boundary (5.11b)

An interesting feature of this model is that the whisker/resistive coating case can be thought of as a limiting case to the whisker/conductive matrix case, when the conductivity is confined to a small region around the fiber. The same governing equations would still apply, except σ_{cm} is zero and the electric boundary condition is

$$(\phi_2 - \phi_1) = R_c \int_A \dot{D}_z \, dA \tag{5.11c}$$

where ϕ_1 and ϕ_2 are the potentials at the ends of the fiber and R_c the coating resistance.

There are two complicating factors. Since the matrix is conductive all around the fiber, there are effectively an infinite number of paths from one end of the fiber to the other and since a piezocomposite has more than one fiber, there is also potential flow from one RVE to another.

The governing equations and boundary conditions do not take this effect into consideration because of how the RVE is defined. This effect is especially important because in a piezocomposite with multiple fibers, there will be flow of charge from one fiber to another. The fiber separation is generally smaller than the fiber length (high volume fraction), and the resistance of a path from one fiber to another will then be smaller than the resistance of a path from one end of the fiber to the other end of the same fiber. Based on the design of the piezocomposite (Fig. 14), the fiber separation is approximately 1/4th the fiber length and flow of charge will be more between different fibers than from end to end of the same fiber. Hence, the formulated electro-micromechanical model is not appropriate for the designed piezocomposite.

The electro-micromechanical is valid if the piezoelectric fiber is shunted using the resistive coating technique. In that case, the potential flow is confined to a path from end to end of the same fiber and the RVE is "representative" of the piezocomposite at the microscopic scale.

5.2. Alternative Models

For the designed whisker piezocomposite, a micro/macromechanical model is formulated in a slightly different manner. A micromechanical model is used to calculate "smeared" effective properties of the piezocomposite from that of its constituents. The effective properties calculated are stiffness, dielectric permittivities, piezoelectric constants and electrical conductivity.

Micromechanical models are available in the literature[23-25] to calculate the above properties. Eqns. (5.3) and (5.8) are then solved for the composite structure (piezocomposite layer and base beam) using the effective properties of the piezocomposite layer and properties of the base beam resulting in modal frequencies and loss factors. A schematic of the model is shown in Figure 18 and the following sections provide details on the above model.

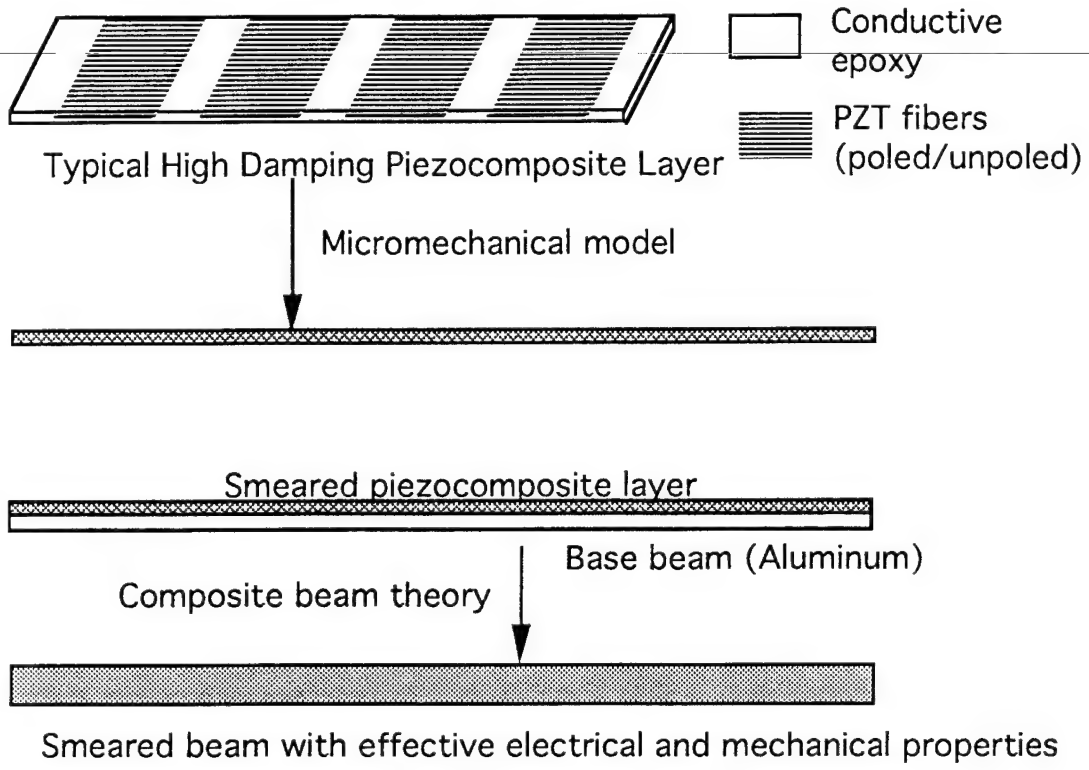

Figure 18. Schematic of Smeared Micromechanical/Dynamic Model

5.2.1. Micromechanical Model

The first step in this model is to calculate the effective properties of the piezocomposite layer. Using relations for two-phase composites with ellipsoidal reinforcement, developed by Benveniste and Dvorak[23], the effective properties of a piezocomposite can be derived as,
Stiffness:

$$
\begin{aligned}
C_{11} &= c_1 C_{11}^1 + c_2 C_{11}^2 - c_1 c_2 \left[C_{12}^1 - C_{12}^2\right]^2 / F \\
C_{12} &= \left[c_1 C_{12}^1 C_{11}^2 + c_2 C_{12}^2 C_{11}^1\right] / F \\
C_{13} &= c_1 C_{13}^1 + c_2 C_{13}^2 + c_1 c_2 \left(C_{13}^2 - C_{13}^1\right)\left[C_{12}^1 - C_{12}^2\right] / F \\
C_{22} &= \left[c_1 C_{11}^1 C_{11}^2 + c_2 C_{11}^2 C_{11}^1\right] / F \\
C_{23} &= c_1 C_{13}^1 + c_2 C_{13}^2 + c_1 c_2 \left(C_{13}^2 - C_{13}^1\right)\left[C_{11}^1 - C_{11}^2\right] / F \\
C_{33} &= c_1 C_{33}^1 + c_2 C_{33}^2 - c_1 c_2 \left[C_{13}^2 - C_{13}^1\right]^2 / F \\
C_{44} &= c_1 C_{44}^1 A^1 + c_2 C_{44}^2 A^2 - c_1 h_1 a^1 - c_2 h_2 a^2 \\
C_{55} &= c_1 C_{44}^1 + c_2 C_{44}^2 \\
C_{66} &= \left(C_{11}^1 - C_{12}^1\right)\left(C_{11}^2 - C_{12}^2\right) / 2\left[c_1 \left(C_{11}^2 - C_{12}^2\right) + c_2 \left(C_{11}^1 - C_{12}^1\right)\right]
\end{aligned}
\qquad (5.12a)
$$

Piezoelectric constants:

$$
\begin{aligned}
e_{31} &= c_1 e_{31}^1 + c_2 e_{31}^2 - c_1 c_2 (e_{31}^1 - e_{31}^2)\left[C_{12}^1 - C_{12}^2\right] / F \\
e_{32} &= c_1 e_{31}^1 + c_2 e_{31}^2 - c_1 c_2 (e_{31}^1 - e_{31}^2)\left[C_{12}^1 - C_{12}^2\right] / F \\
e_{33} &= c_1 e_{33}^1 + c_2 e_{33}^2 - c_1 c_2 (e_{31}^1 - e_{31}^2)\left[C_{13}^1 - C_{13}^2\right] / F \\
e_{15} &= c_1 e_{15}^1 + c_2 e_{15}^2 \\
e_{24} &= c_1 h_1 b^1 + c_2 h_2 b^2 - c_1 C_{44}^1 B^1 - c_2 C_{44}^2 B^2
\end{aligned}
\qquad (5.12b)
$$

Dielectric permittivities:

$$
\begin{aligned}
\kappa_{11} &= -c_1 \kappa_{11}^1 - c_2 \kappa_{11}^2 \\
\kappa_{22} &= -c_1 \kappa_{11}^1 b^1 - c_2 \kappa_{11}^2 b^2 + c_1 h_1 B^1 + c_2 h_2 B^2 \\
\kappa_{33} &= -c_1 \kappa_{33}^1 - c_2 \kappa_{33}^2 - c_1 c_2 (e_{31}^1 - e_{31}^2)^2 / F
\end{aligned}
\qquad (5.12c)
$$

where:

$$F = c_2 C_{11}^1 + c_1 C_{11}^2$$

$$F' = \left[\left(c_1 C_{44}^2 + c_2 C_{44}^1\right)\left(c_1 \kappa_{11}^2 + c_2 \kappa_{11}^1\right) + \left(c_1 e_{15}^2 + c_2 e_{15}^1\right)^2\right]$$

$$A^1 = \left[\left(c_1 \kappa_{11}^2 + c_2 \kappa_{11}^1\right) C_{44}^2 + \left(c_1 e_{15}^2 + c_2 e_{15}^1\right) e_{15}^2\right] / F'$$

$$A^2 = \left[\left(c_1 \kappa_{11}^2 + c_2 \kappa_{11}^1\right) C_{44}^1 + \left(c_1 e_{15}^2 + c_2 e_{15}^1\right) e_{15}^1\right] / F'$$

$$a^1 = c_2\left[e_{15}^2 C_{44}^1 - e_{15}^1 C_{44}^2\right] / F'$$

$$a^2 = c_1\left[e_{15}^1 C_{44}^2 - e_{15}^2 C_{44}^1\right] / F'$$

$$B^1 = c_2\left[\kappa_{11}^2 e_{15}^1 - \kappa_{11}^1 e_{15}^2\right] / F'$$

$$B^2 = c_1\left[\kappa_{11}^1 e_{15}^2 - \kappa_{11}^2 e_{15}^1\right] / F'$$

$$b^1 = \left[\left(c_1 C_{44}^2 + c_2 C_{44}^1\right) \kappa_{11}^2 + \left(c_1 e_{15}^2 + c_2 e_{15}^1\right) e_{15}^2\right] / F'$$

$$b^2 = \left[\left(c_1 C_{44}^2 + c_2 C_{44}^1\right) \kappa_{11}^1 + \left(c_1 e_{15}^2 + c_2 e_{15}^1\right) e_{15}^1\right] / F'$$

c_1, c_2 = volume fractions of phases 1 and 2

In the above relations, both phases 1 and 2 are piezoelectric and transversely isotropic. For the piezocomposite, phase 1 is the piezoelectric fiber (transversely isotropic) and phase 2 is the conductive matrix (isotropic). To calculate effective conductivity of the piezocomposite, the fiber is assumed to be non-conductive. In that case, the effective volume fraction of the filler is recalculated for the piezocomposite. The percolation curve[13,14] (relating filler volume fraction to conductivity) is used to calculate the effective piezocomposite conductivity.

The major difference between this micromechanical model and that outlined in the previous section is that the electrical interaction between the conductive matrix and the piezoelectric fiber is not taken into account, while developing the micromechanical relations. Instead the structure is assumed to be a smeared conductive piezocomposite material with effective properties given by the above set of equations.

5.2.2. Smeared Structural Dynamic Model

Using the effective piezocomposite properties, Eqns. (5.3) and (5.8) can be rewritten for a composite beam (based on composite beam theory) as,

$$A_{33}\frac{d^2u^\circ}{dx^2} - B_{33}\frac{d^2w}{dx^2} + e_{33}t\frac{d^2\phi}{dx^2} - \rho\frac{d^2u^\circ}{dt^2} = 0$$

$$D_{33}\frac{d^4w}{dx^4} - B_{33}\frac{d^3u^\circ}{dx^3} - e_{33}h\frac{t}{2}\frac{d^3\phi}{dx^3} + \rho\frac{d^2w}{dt^2} = 0 \qquad (5.13a\text{-}c)$$

$$\frac{d}{dt}\left\{e_{33}\frac{d^2u}{dx^2} - \varepsilon_{33}\frac{d^2\phi}{dx^2}\right\} - \sigma_c\frac{d^2\phi}{dx^2} = 0$$

where

$$u(x,t) = u^\circ(x,t) - z\frac{dw}{dx}$$

$$w = w(x,t)$$

$$\phi = \phi(x,t)$$

$$A_{ij} = \int_{z_k}^{z_{k+1}} Q_{ij}^k\, dz \qquad B_{ij} = \int_{z_k}^{z_{k+1}} Q_{ij}^k\, z dz$$

$$D_{ij} = \int_{z_k}^{z_{k+1}} Q_{ij}^k\, z^2 dz$$

and h is the base beam thickness and t the thickness of the piezocomposite layer. Q_{ij}^k are the reduced stiffness of kth layer in the structure. There is axial-bending coupling (B term) because the piezocomposite layer is bonded to only side of the base beam. If the base beam has a single high damping piezocomposite layer on either the top or the bottom surface, the resultant beam is unsymmetric. If two layers are used, one on the top and one on the bottom, the beam becomes symmetric (assuming both layers are similar). If the beam is unsymmetric, there is axial-bending coupling as reflected by a non-zero B matrix. If the beam is symmetric, B is zero and the first two equations are uncoupled. If a bending load is applied to a beam, in the unsymmetric case both u° and w are non-zero, whereas in the symmetric case, u° becomes zero (mid-plane axial deformation). In the unsymmetric case, the axial displacement in the piezocomposite layer is a function of both u°, z and w. In the symmetric case, it is function of z and w alone.

The displacement in the piezoelectric layer can be expressed as,

Unsymmetric Case

$$u(x,t) = u^\circ(x,t) - z\frac{dw}{dx}$$

$$w = w(x,t)$$

Symmetric Case

$$u(x,t) = -z\frac{dw}{dx}$$

$$w = w(x,t)$$

z is the distance of the mid plane of the piezocomposite layer from the mid plane of the beam. Eqns. (5.13) are derived from Eqns. (5.3) and (5.8) using composite beam theory. The designed composite structure (Fig. 14) is treated as a 2-layer composite laminate with the first layer being the base beam and the second layer the piezocomposite layer.

Eqns. (5.13) are the general axial/flexural vibration equations of the composite structure. Note that there is an explicit electrical equation in this formulation, which would not have been there if the micro-electromechanics model was used. The piezoelectric constants, permittivities and conductivity in Eqns (5.13) are effective properties of the piezocomposite layer derived in the previous section.

5.2.3. Solution of smeared beam dynamic model

The derived governing equations can be solved for either axial or flexural vibration. For flexural vibration, Eqns. (5.13) can be reduced to a single equation in the frequency domain, as follows

$$\left[\overline{D}+\overline{e}\left(\frac{B_{33}}{A_{33}}-\frac{h}{2}\right)\frac{e_{33}^2 i\omega}{\sigma_c+\varepsilon_{33} i\omega}\right]\frac{d^4 w}{dx^4} - \omega^2 \rho\, w = 0 \tag{5.14}$$

$$\overline{D} = D_{33}A_{33} - B_{33}^2 \tag{5.15}$$

$$\overline{e} = e_{33} t\left\{B_{33} - \frac{A_{33} h}{2}\right\} \tag{5.16}$$

Eqn. (5.14) is of the form $[K - \omega^2 M] = 0$, where K is complex and frequency dependent. The frequency dependence is induced by the conductivity of the composite structure. To calculate the loss factor for the structure, the complex stiffness term is rewritten as

$$D = \overline{D}+\overline{e}\left(\frac{B_{33}}{A_{33}}-\frac{h}{2}\right)\frac{e_{33}^2 i\omega}{\sigma_c+\varepsilon_{33} i\omega} = D' + iD'' \tag{5.17}$$

where

$$D' = \overline{D}+\overline{e}\left(\frac{B_{33}}{A_{33}}-\frac{h}{2}\right)\frac{\varepsilon_{33} e_{33}^2 \omega^2}{\sigma_c^2+(\varepsilon_{33}\omega)^2}$$

$$D'' = \overline{e}\left(\frac{B_{33}}{A_{33}}-\frac{h}{2}\right)\frac{\sigma_c e_{33}^2 \omega^2}{\sigma_c^2+(\varepsilon_{33}\omega)^2}$$

The structural loss factor is a function of frequency and is given by

$$\eta = \frac{D''}{D'} = \frac{\bar{c}\,\Delta\,\omega}{1+(\bar{c}\Delta\tau+\tau^2)\omega^2} \tag{5.18}$$

and

$$\bar{c} = \frac{\bar{e}}{\bar{D}}\left(\frac{B_{33}}{A_{33}} - \frac{h}{2}\right) \qquad \Delta = \frac{e_{33}^2}{\sigma_c} \qquad \tau = \frac{\varepsilon_{33}^2}{\sigma_c}$$

The structural loss factor is maximum for a particular frequency, which is

$$\omega = \sqrt{\frac{1}{\bar{c}\Delta\tau+\tau^2}} \tag{5.19}$$

From the above equation, we can determine the optimum structural properties which will give the maximum loss factor. The goal is to match the structural frequency in the required mode with the frequency given by Eqn. (5.19), so that maximum loss is obtained at the desired mode.

5.2.4. Model Deficiencies

The major assumption in the smeared model, is that the effective properties of the piezocomposite derived using the micromechanical model, completely describe the electromechanical behavior of the composite. This is not exactly true, especially considering the geometry and layout of the piezocomposite layer.

At the microscopic level, the piezocomposite layer has discontinuous properties. The properties vary based on the arrangement or packing of the fibers within the piezocomposite. Along the length direction of the piezocomposite, there are 2 distinctly different regions as shown in Figure 19 below.

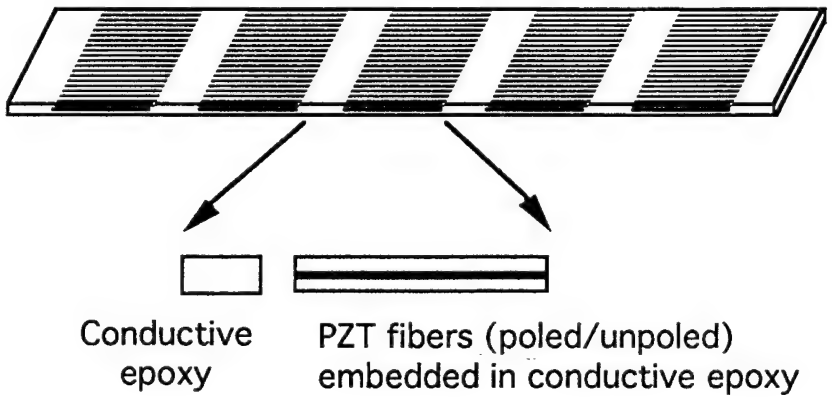

Figure 19. Typical High Damping Piezocomposite Layer

The smeared model fails to address the following two issues:

- The presence of more than one conduction path within the matrix. Based on the fiber packing, the resistive path from one fiber end to the adjacent fiber can be smaller than that from end to end of the same fiber. In that case, a larger part of the conduction occurs from one fiber to the adjacent fiber. The smeared model predicts one characteristic resistance irrespective of fiber packing.

- The local variations in electrical and mechanical properties. The conductive epoxy part has properties that are widely different from those within the fiber part resulting in different displacements and potentials. Cases of non-uniform strain along the length and through the thickness not addressed as the micromechanical model is based on a uniform fields approach.

An approximate equivalent circuit comparison between the smeared beam model and the actual behavior is shown in Fig. 20, and reveals some insight into the physics of the problem of multiple conduction paths.

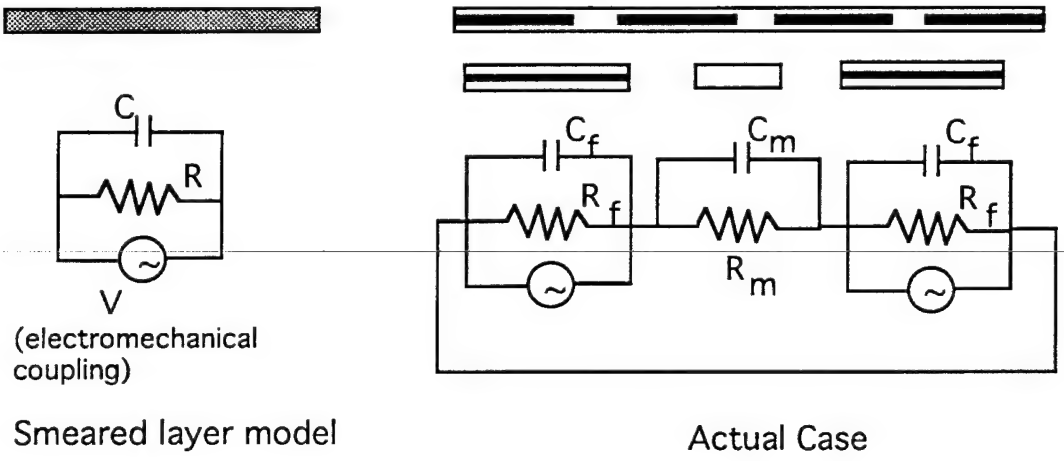

Figure 20. Approximate Equivalent Circuit Comparison

Of the many possible conduction paths within the piezocomposite layer, the two main conduction paths are: the end of one fiber to the end of an adjacent fiber and from end to end of the same fiber. If the ends of the piezocomposite layer are not electrically connected, there will be no conduction from end of one fiber to the end of the adjacent fiber. The only conduction path in that case is from end to end of the same fiber. If the ends of the piezocomposite are electrically

connected, there are now two main conduction paths. In such a case, the loss factor will show 2 peaks (one for each conduction path). It is expected that separation of the two phenomena into different regimes will have some bearing on the modal loss factors and frequencies of the beam system.

Since the smeared beam model does not capture the above mentioned behavior of the piezocomposite (gives an averaged view of the structure), a different type of solution technique is needed. The major advantage of the smeared mode is its simplicity and ease of solution. Due to the material property discontinuity along the length of the structure, however, the finite element method seems to be the best choice for modeling the composite structure.

5.3. Micromechanics Based Finite Element Model

Finite element (FE) models[26-30] are well suited to model structural discontinuities. The material property discontinuities that are present in the piezocomposite layer can be easily handled with FE models by defining two types of elements: a piezoelectric element and a conductive element. The piezoelectric elements model the piezoelectric fibers within the composite and the conductive elements model the matrix. A schematic of a typical model is shown below,

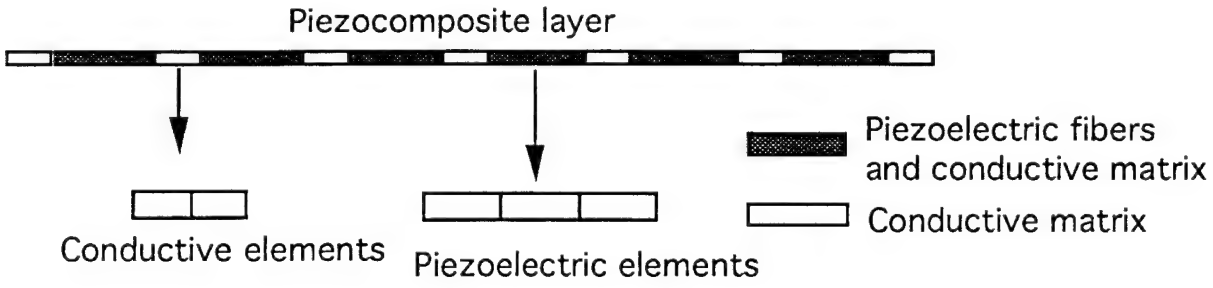

Figure 21. Schematic of Discretization of Piezocomposite Structure

The micromechanical model described in Sec. 5.2.1 is used to determine the material properties of each element type. For the conductive matrix segment, the effective properties are calculated using micromechanical relations available in the literature[31]. Since the filler volume fraction in the epoxy matrix is fairly high (approximately 10-15%) it cannot be treated as a dilute suspension. Hence, the micromechanical relations are not exact and can only predict bounds for the elastic properties. Conductivity of the matrix is calculated from the percolation curve[13,14]. For the piezoelectric segment, effective elastic, piezoelectric and dielectric properties are derived using the fiber volume fraction and the fiber and matrix properties. Conductivity of this element is calculated based on the area fraction of the matrix in the cross-section of the element.

A Galerkin type finite element formulation was used to derive the discretized equations of motion from the governing differential equations (Eqns. (5.3) and (5.8)). The second order equations of motion were reduced to first order form using a state-space type formulation and solved for the eigenvalues of the system. The following sections provide details about the finite element formulation and the discretized equations.

5.3.1. The Element

The element used is a three noded 1-D C^1 continuous element. It has a total of 10 degrees of freedom and is shown in the figure below.

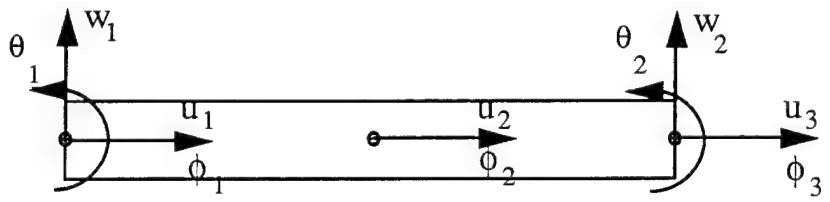

Figure 22. A Single Element showing the Degrees of Freedom

The displacements are related to the nodal degrees of freedom by the shape functions as follows,

$$\begin{Bmatrix} u \\ w \\ \phi \end{Bmatrix} = \begin{bmatrix} N_u & N_w & N_\phi \end{bmatrix} \begin{Bmatrix} u_i \\ w_i \\ \phi_i \end{Bmatrix} \tag{5.20}$$

where

$$N_u = \left[1 - \frac{3x}{L} + \frac{2x^2}{L^2} \quad \frac{4x}{L} - \frac{4x^2}{L^2} \quad -\frac{x}{L} + \frac{2x^2}{L^2} \right]$$

$$N_w = \left[1 - \frac{3x^2}{L^2} + \frac{2x^3}{L^3} \quad x - \frac{2x^2}{L} + \frac{x^3}{L^2} \quad \frac{3x^2}{L^2} - \frac{2x^3}{L^3} \quad -\frac{x^2}{L} + \frac{x^3}{L^2} \right]$$

$$N_\phi = \left[1 - \frac{3x}{L} + \frac{2x^2}{L^2} \quad \frac{4x}{L} - \frac{4x^2}{L^2} \quad -\frac{x}{L} + \frac{2x^2}{L^2} \right]$$

and L is the length of the element and w_i includes w and θ.

The chosen shape functions are C^1 continuous, i.e. at each node, both the displacement and the slope are continuous. Shape functions for w are one power higher than that of u and ϕ because, u is proportional to dw/dx and u and ϕ are directly proportional.

Using these shape functions, the stiffness, damping and mass matrices of the element can be calculated. Due to the simple algebraic form of the shape functions, the matrices can be explicitly derived.

5.3.2. Discretized equations of motion

Using the Galerkin type formulation the governing equations of the beam can be discretized to the following form,

$$\begin{bmatrix} M_u & 0 & 0 \\ 0 & M_w & 0 \\ 0 & 0 & 0 \end{bmatrix} \{\ddot{q}\} + \begin{bmatrix} 0 & 0 & 0 \\ 0 & 0 & 0 \\ C_{pu} & -C_{pw} & -C_{p\phi} \end{bmatrix} \{\dot{q}\} + \begin{bmatrix} K_u & -K_{uw} & K_{eu} \\ -K_{uw}^T & K_w & -K_{ew} \\ 0 & 0 & -K_{\sigma_c} \end{bmatrix} \{q\} = \{Q\} \tag{5.21}$$

where

$$M_u = \int_0^L [N_u]^T \rho [N_u] dx \qquad M_w = \int_0^L [N_w]^T \rho [N_w] dx$$

$$K_u = \int_0^L [N_{u,x}]^T A_{33} [N_{u,x}] dx \qquad K_w = \int_0^L [N_{w,xx}]^T D_{33} [N_{w,xx}] dx$$

$$K_{uw} = \int_0^L [N_{u,x}]^T B_{33} [N_{w,xx}] dx \qquad K_{\sigma_c} = \int_0^L [N_{\phi,x}]^T \sigma_c t [N_{\phi,x}] dx$$

$$K_{eu} = \int_0^L [N_{u,x}]^T te_{33} [N_{\phi,x}] dx \qquad K_{ew} = \int_0^L [N_{w,xx}]^T h\frac{t}{2} e_{33} [N_{\phi,x}] dx$$

$$C_{pu} = \int_0^L [N_{\phi,x}]^T e_{33} t [N_{u,x}] dx \qquad C_{pw} = \int_0^L [N_{\phi,x}]^T e_{33} h\frac{t}{2} [N_{w,xx}] dx$$

$$C_{p\phi} = \int_0^L [N_{\phi,x}]^T \varepsilon_{33} h [N_{\phi,x}] dx$$

where h is base beam thickness and t is the piezocomposite layer thickness.

All the above matrices can be explicitly derived for the element because of the simple algebraic form of the shape functions. Matrices with subscripts "eu", "ew", "uw" refer to coupling terms. The first two subscripts are electromechanical coupling with axial deformation and bending deformation respectively. The last subscript refers to axial-bending coupling (the B terms). In special cases some of the matrices are zero and can simplify the problem. The damping matrix shows only the terms due to shunting. Damping due to the polymer matrix or the aluminum beam can simply be included by including the terms in the appropriate part of the damping matrix.

The Q matrix is the nodal dynamic forcing matrix. In free vibration cases, Q is zero. If a dynamic force is applied to the beam, Q is non-zero and is the nodal load vector.

If the conductivity of the system is zero, the potential equation is no longer dynamic and becomes static and there is no damping. The resultant eigenvalues are complex with zero real parts (zero damping).

Using a state-space type approach, the discretized dynamic equations can be written in the following form,

$$\underbrace{\begin{bmatrix} M & 0 & 0 \\ 0 & I & 0 \\ 0 & C_p & -C_{p\phi} \end{bmatrix}}_{\text{A matrix}} \begin{Bmatrix} \ddot{q}_u \\ \dot{q}_u \\ \dot{q}_\phi \end{Bmatrix} + \underbrace{\begin{bmatrix} 0 & K & K_e \\ -I & 0 & 0 \\ 0 & 0 & -K_{\sigma_c} \end{bmatrix}}_{\text{B matrix}} \begin{Bmatrix} \dot{q}_u \\ q_u \\ q_\phi \end{Bmatrix} = \{Q\} \tag{5.22}$$

where

$$M = \begin{bmatrix} M_u & 0 \\ 0 & M_w \end{bmatrix} \qquad K = \begin{bmatrix} K_u & -K_{uw} \\ -K_{uw}^T & K_w \end{bmatrix}$$

$$C_p = \begin{bmatrix} C_{pu} & -C_{pw} \end{bmatrix} \qquad K_e = \begin{bmatrix} K_{eu} \\ -K_{ew} \end{bmatrix}$$

$$q_u{}^T = \{u_i \quad w_i \quad \theta_i\}$$

and I is an identity matrix. The eigenvalue problem of the above system of equations is of the form $Aq = -\lambda Bq$ where a λ is a diagonal matrix of eigenvalues. The derived eigenvalue is complex and of the form

$$\lambda = -\varsigma\omega \pm i\omega\sqrt{1 - \varsigma^2} \tag{5.23}$$

where ω is the resonant frequency and ζ is the damping ratio ($\eta/2$) for small η.

5.3.3. *Comparison of Predictions with Smeared Model*

The above finite element model was tested by comparing the maximum loss factor predictions with those of the smeared 1-D analytical model.

The following constituent properties were used as a test case,

Epoxy:	E_L = 4.0 GPa	G_{LT} = 1.45 GPa	v_m = 32%	
Filler	E_L = 100 GPa	G_{LT} = 38.5 GPa	v_{fil} = 48%	
PZT5A	C_{33} = 121 GPa	e_{33} = 15.8	$e_{33} = 7.345 \times 10^{-9}$	v_{pzt} = 20%

gives the following effective properties,

$$E_{33} = 20.87 - 47.56 \text{ GPa}$$
$$e_{33} = 3.709 - 3.57$$
$$e_{33} = 1.423 - 1.426 \times 10^{-9}$$

for the smeared piezocomposite layer.

The micromechanical model predicts bounds for the effective properties and not exact values. Using the upper and lower bounds as the limiting cases, maximum possible loss factors for the first mode were predicted as follows,

$$\eta_{low} = 8.62\% \ (8.98) \qquad \eta_{high} = 19.14\% \ (20.95)$$

The FE model predictions are given in parentheses and compare well with the predictions of the analytical 1-D smeared model. Several different cases were examined to compare the FE model predictions with the analytical model and are listed in the Table 5.1. The FE predictions compare very well with analytical predictions, with increasing differences with higher loss factors.

5.3.4. *Whisker/Thin Film Resistor Case*

The discretized dynamic equations, Eqn. (5.22), are for the whisker/conductive matrix case. In order to apply the discretized equations to the thin film case, they have to be slightly modified in the following manner:

The thin film is treated as a separate layer of thickness t_f, and is assumed to be only resistive or conductive in nature. It is assumed that the thin film does not affect the mechanical, electromechanical or dielectric behavior of the structure. The total thickness of the composite beam

is then h+ t + t_f, where h is the thickness of the base beam and t the thickness of the piezocomposite layer. This modifies the K_{σ_c} matrix in Eqn. (5.21) to,

$$K_{\sigma_c} = \int_0^L \left[N_{\phi,x}\right]^T \sigma_c t_f \left[N_{\phi,x}\right] dx \qquad (5.24)$$

and all the other terms and equations remain the same.

Table 5.1 Comparison of First Mode Loss Factor Predictions Between 1-D Smeared Model and Finite Element Model

Case Number	1-D Smeared Model (%)	Finite Element Model (%)
1	19.14	20.95
2	8.62	8.98
3	21.7	24.03
4	10.37	10.92
5	23.9	26.8
6	12.5	13.3
7	12.2	12.97
8	4.62	4.73
9	14.5	15.54
10	5.71	5.88
11	16.71	18.1
12	7.13	7.38

Cases 1-6 are for 20% PZT volume fraction and represent upper/lower bounds for 3 different combinations of filler/matrix volume fractions.

Cases 7-12 are for 10% PZT volume fraction.

5.4. Passively Damped Structure Design Using Finite Element Model

Using the finite element based dynamic model, critical parameters affecting structural frequencies and damping can be identified. The critical parameters are volume fraction of the piezoelectric whiskers, shunt resistance value and the geometry of the piezocomposite beam. Geometry includes whisker packing system, piezocomposite and base beam dimensions and in the thin film case, film thickness and location of the piezocomposite sample along the base beam.

The effect of the above parameters on structural damping was determined by using the model to estimate variation in structural damping over a range of values for each parameter. Results are presented and discussed in a later chapter. The objective of this analysis is to determine the parameters for optimum damping at a specified mode.

5.4.1. Whisker/Conductive Epoxy Case

Beam parameters for optimum damping in second bending mode are,

2-layer composite beam :
One piezocomposite layer
One Aluminum layer

Beam length = 8.1 cm
Beam width = 1.0 cm
Beam thickness :
Piezocomposite layer = 200 μm
Base Aluminum beam = 200 μm

Piezocomposite layer:
PZT volume fraction = 20%
PZT fiber (l/d) = 100
PZT fiber diameter = 120 μm
Distance between fiber (lengthwise) = 0.3 cm
Matrix Conductivity = 1e-5 Ω^{-1} m^{-1}
(optimized for mode 2)

Piezocomposite layer "reinforcing" Aluminum beam
Adhesive: Superglue
Apply pressure for 5-10 mins while adhesive cures.
Adhesive layer thickness is small (<= 1 mil)

5.4.2. Whisker/Thin Film Resistor Case

Beam paramaters for optimum damping in second bending mode are,

Composite beam :

One Aluminum layer
2 shunted piezocomposite samples bonded at the root
Beam length = 8.1 cm
Beam width = 1.0 cm
Beam thickness = 200 μm

Piezocomposite sample:

Dimensions = 1.2cm x 0.6cm x 200 μm
PZT volume fraction = 40%
PZT fiber (l/d) = 100
PZT fiber diameter = 120 μm
Thin film resistance - to be determined exactly with external shunt resistor

Piezocomposite sample bonded to aluminum beam
Adhesive: Superglue
Apply pressure for 5-10 mins while adhesive cures.
Adhesive layer thickness is small (<= 1 mil)

6. EXPERIMENTAL WORK

In order to validate the theoretical models for piezocomposites, the designed piezocomposite structure was manufactured and tested. The following sections describe manufacturing procedures and related issues for whisker/conductive matrix and whisker/thin film piezocomposites.

6.1. Constituent Materials

The main constituent materials involved in piezocomposite manufacture are PZT-5H whiskers and epoxy resin HD-85J. The filler, for the conductive matrix case, is a Sn:SnO_2 mixture and the thin film, in the thin film resistor case, is a SiC film.

The PZT-5H whiskers were made by chopping 8-10 cm long, 120 μm diameter fibers (supplied by CeraNova) into 1.2 cm long segments (100 aspect ratio). In the thin film shunted piezocomposite case, unpoled fibers were chopped into whiskers and poled after the piezocomposite was manufactured. The long fibers were poled using a continuous poling technique described in the previous chapters. Approximately 150 long fibers of length between 8-10 cm were poled using the continuous poling technique. This limited the number of available poled whiskers to approximately one thousand. Because a large number of whiskers are needed to obtain a reasonable fiber volume fraction (> 10%) in the piezocomposite, the number of specimens that could be manufactured was very limited and required careful planning.

The matrix is a HD-85J epoxy resin provided by Fiber Materials Inc. It consists of two parts, the epoxy resin and the hardener, which are mixed at the ratio of 71.215%:28.785% by

weight. The two parts are added and mixed till the mixture is homogenous and degassed under full vacuum for approximately 15 mins. to remove air bubbles. The cure cycle involves heating the resin at 80°C for 2 hours followed by heating to 100°C for 3 hours.

6.2. Conductive Matrix

The filler material used was a $Sn:SnO_2$ mixture, with particle size smaller than 0.5 μm. Figure 5.1 is a schematic of the conductive matrix preparation procedure. After preparation of

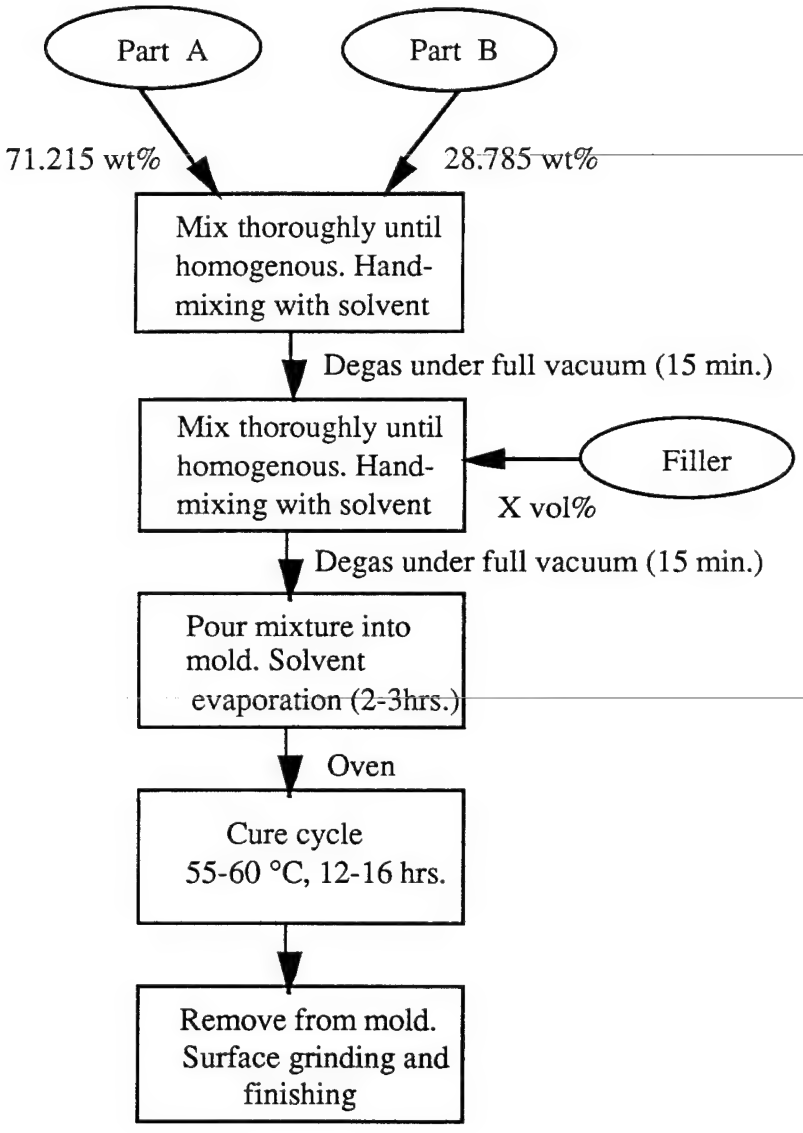

Figure 23. Flow Chart of Conductive Matrix Preparation Procedure

the epoxy resin, a known weight of filler material was added to it and hand-mixed. Since the filler volume fractions required were of the order of 10-15%, the viscosity of the resulting mixture was high, and a solvent was necessary. Toluene was used as the solvent to reduce viscosity and improve mixing of the filler particles with the matrix. After mixing, the mixture was degassed under vacuum once again, to remove air bubbles. A simple aluminum mold (Figure 24) was prepared and coated with a release agent. The mixture was poured into the mold and a slow, low temperature cure cycle (55-60 °C for 12-16 hrs.) was used to cure the filler epoxy mixture.

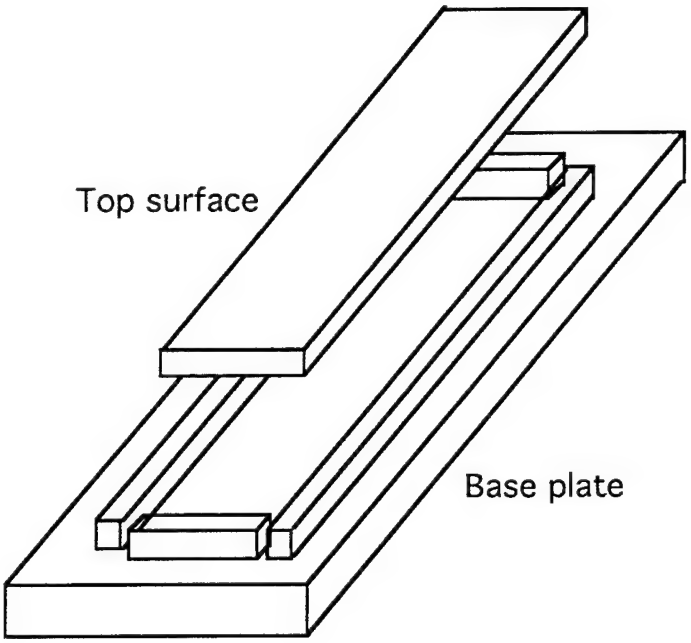

Figure 24. Schematic of the Mold for Piezocomposite Layer

Initial conductive epoxy samples showed significant levels of porosity. This was due to the presence of the solvent, high viscosity of the filler epoxy mixture and trapped air during the mixing process. The problem of porosity was solved by using vacuum to degas the mixture and reducing the mixture viscosity by adding more solvent (toluene). While reducing viscosity of the mixture and degassing removes trapped air very effectively, the mixture cannot be cured without allowing the toluene to evaporate. If the mixture is cured without allowing enough time for the toluene to evaporate, several pockets of trapped gas are formed within the sample during cure. Therefore, after degassing the mixture under vacuum, the mixture was poured into the mold and allowed to sit in a ventilated hood for 2-3 hrs. to facilitate evaporation of the solvent. The mold was then placed in an oven at 55-60 °C for 12-16 hrs (overnight) for the epoxy to cure.

Property characterization of the resultant conductive matrix was performed to determine its electrical resistivity and mechanical properties. Elastic stiffness was characterized by bonding a conductive matrix layer to an aluminum base beam and performing a simple flexure test. A strain gage was used to measure strain on the beam top surface for an applied bending load and the elastic properties calculated from composite beam theory. Electrical resistivity characterization techniques are described in a later section. Results of the characterization tests are presented in the next chapter.

6.3. Whisker/Conductive Matrix Piezocomposite

As mentioned in the earlier section, PZT-5H whiskers were made by chopping 8-10 cm long poled PZT-5H fibers into segments of length 1.2 cm (aspect ratio 100). The initial design of the piezocomposite involved manufacturing a piezocomposite layer of dimensions 8.5 cm x 1 cm x 200 μm, which is one whisker layer thick. The whiskers were to be placed along the length with a gap of 0.3 cm between adjacent segments and approximately 40 whiskers were to be placed along the width. Figure 25a shows a schematic of the piezocomposite configuration and Figure 25b a schematic of the manufacturing procedure.

The mold was coated with release agent and a thin layer of conductive epoxy was painted onto the mold base plate. PZT-5H whiskers were placed by hand onto the layer of epoxy in the mold according to the design configuration. Before each whisker was placed in the mold, the ends were electroded by dipping in air-dried silver solution. Also, the poling direction of each whisker was carefully noted, so that the poling direction of all the whiskers in the composite was the same. After placing all the whiskers within the layer of epoxy in the mold, a second layer of epoxy was carefully applied to cover the fibers. After placing the mold in a ventilated hood for 2-3 hrs, an aluminum top surface was applied (to provide uniformity of specimen thickness) and mold placed in an oven for overnight cure at 55-60 °C.

Due to the limited availability of piezoelectric whiskers, silver wire segments of the same diameter were used in initial trial runs. The first piezocomposite layer developed was much thicker than expected resulting in a fiber volume fraction of 2.5%. The top and bottom surfaces were ground using coarse and fine grid paper to reduce the thickness. Grinding was not very successful in reducing the layer thickness for several reasons. Due to the high viscosity of the conductive epoxy, it was impossible to place all the whiskers in the same cross-sectional plane, during hand-layup. If the whiskers are not in the same cross-sectional plane, the design thickness of 200 μm cannot be achieved without damage to the fibers that are out of the plane, as shown in Fig. 26. Also, grinding the conductive epoxy was harder and time consuming because of the presence of the filler particles.

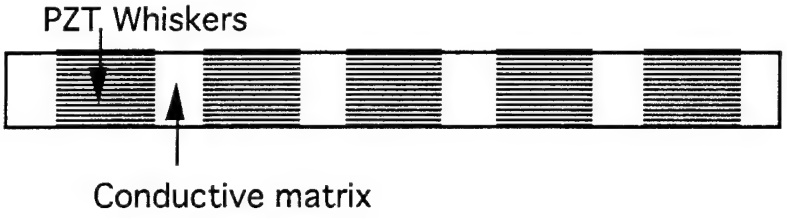

Figure 25a. Schematic of Piezocomposite Layer

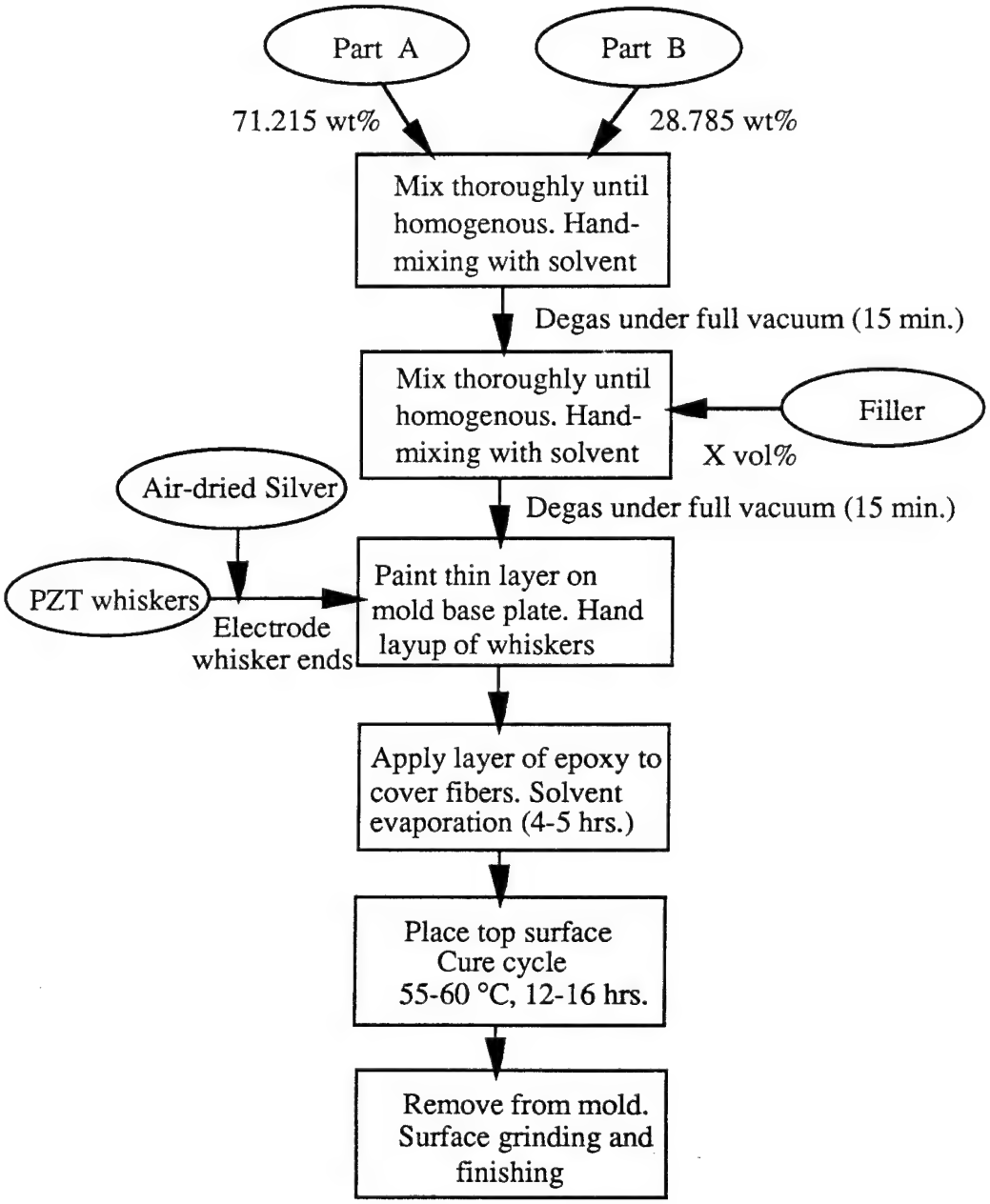

Figure 25b. Flow Chart for Whisker/Conductive Matrix Piezocomposite Preparation

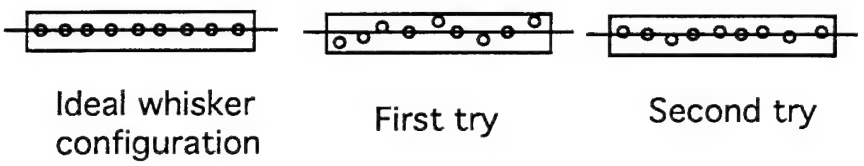

Figure 26. Whisker Location in the Cross-Section of Layer

In order to manufacture the piezocomposite layer in a near net shape, the viscosity of the conductive matrix was reduced significantly by adding toluene. The advantage of reducing viscosity is that a much thinner bottom and top epoxy layer can be applied. Also, low viscosity allows the whiskers to "settle" consistently within the epoxy resulting in most of the whiskers being in the same cross-sectional plane. The main disadvantage of this step is that the amount of time needed to allow the solvent to evaporate is greater. After placement of fibers and applying the top layer of epoxy, the mold was allowed to sit in a ventilated hood for 4-5 hrs. The top surface of the mold was then applied and C clamps were used to apply pressure to the top and the base of the mold. The mold was placed in the over at 55-60°C for overnight cure.

The resulting piezocomposite layer was very close to the desired dimensions and only needed light grinding to achieve the final shape (8.5 cm x 1 cm x 200 μm). For dynamic testing to determine passive damping improvements, the piezocomposite layer was bonded to an aluminum base beam using an adhesive (Krazy-Glue). Care was taken to minimize the bonding layer thickness, so that damping contributions to the structure, due to that layer were small. Also, a sample of the same conductive epoxy was prepared for resistivity characterization. It should be noted at this point, that it is not possible to characterize d_{33} or the dielectric constant of the piezocomposite layer.

6.4. Whisker/Thin Film Resistor Piezocomposite

The preparation procedure for this configuration is very similar to the whisker/conductive matrix case and is shown schematically in Figure 27. After preparing the epoxy and the mold, a thin layer of pure epoxy was applied to the mold base plate. While keeping track of the poling direction, piezoelectric whiskers were placed by hand in the layer of epoxy. Since there is no filler in the epoxy, the viscosity of the epoxy is low and the whiskers "settle" uniformly towards the bottom of the epoxy layer. The whiskers could also be carefully moved close to each other and tight packing of whiskers was possible. The mold base plate was placed in a hood for 2-3 hrs. and cured overnight at 55-60°C. After cure, the sample was removed and the top surface was lightly ground to achieve the final dimensions. Grinding of pure epoxy was much easier and faster compared to the conductive epoxy case and because pure epoxy was used, porosity and viscosity are no longer significant problems.

The initial design configuration (Figure 28) of the piezocomposite sample called for dimensions of 1.2 cm x 0.7 cm x 200 μm. These dimensions were easy to achieve and resulted in fiber volume fractions between 32-35%. Each sample had between 42-45

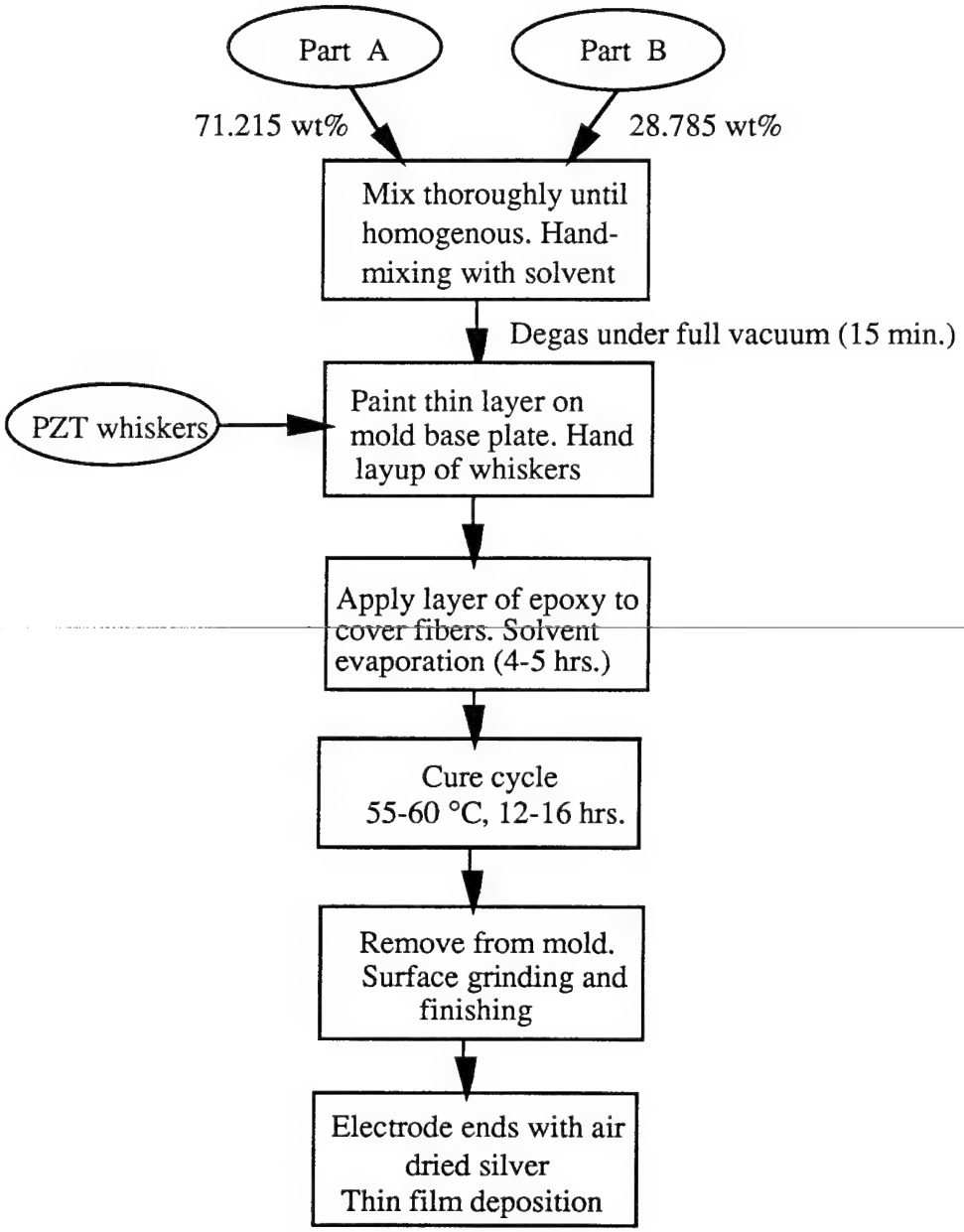

Figure 27. Flow Chart for Whisker/Thin Film Piezocomposite Preparation

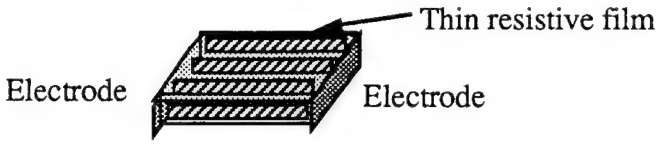

Figure 28. Schematic of Thin Film Piezocomposite Sample

fibers along the width. The sample was electroded by applying air-dried silver to the ends (along the length). Thin silver wires were bonded to the electroded ends using conductive silver epoxy for electrical characterization tests.

For the case where unpoled whiskers were used instead of poled whiskers, the whiskers were poled using a standard poling technique, after the sample was prepared. The sample was immersed in an oil bath at room temperature and an electric field (~10KV/cm) was applied across the electrodes of the sample for approximately 1 min. For these samples, the fiber volume fraction was higher, ranging from 39-42%. For these piezocomposite samples, it is possible to characterize the electromechanical and dielectric properties. The next section describes these procedures in detail. Measuring elastic properties is not possible due to the geometry and small size of the samples.

A thin SiC film was deposited on the top surface of the sample, between the electroded ends, to serve as the shunt resistor. While the theoretical model provides an estimate of the required resistance for peak damping, the exact resistance can be determined by shunting the sample with varying external shunt resistors and measuring structural damping. A film of the required thickness can then be deposited on the sample. The following section briefly describes the deposition technique and setup.

6.4.1. Thin Film Deposition Technique

Amorphous-hydrogenated silicon carbide films were deposited by dc-magnetron sputtering of a Hexoloy SC silicon carbide target in an argon/hydrogen plasma. The target, supplied by Carborundum Company was two inches in diameter and one-eight inch thick.

The deposition system was evacuated to a base pressure of ~2×10^{-7} Torr (overnight pumping) with a 1500 liter./second turbomolecular pump backed with a 36.7 cfm mechanical pump. Residual gas analysis of the chamber indicated that the water vapor and oxygen partial pressure were < 5×10^{-8} Torr. The target to substrate distance was 60mm and the total gas pressure was 10 millitorr, thus optimizing the bombardment of the growing films by sputtering atoms and the reflected neutrals (plasma) from the target. Argon and hydrogen gases (99.999% purity) were

introduced into the chamber independently by means of separate mass flow controllers operated by an MKS 147 Multi-Gas controller. The target power was fixed at 100 watts by a dc power supply.

The substrates were placed on a rotatable platform that allowed up to six different depositions to be conducted with a single pumpdown. A shield with a rectangular opening was positioned between the target and the substrate platform and the substrates were rotated under the opening. A slight increase in temperature (~40°C) of the growing film was observed during deposition due to the bombardment process and the heat of condensation of the evolving film. In order to characterize the thin film, films of varying thicknesses were deposited on four pure epoxy substrates. Resistivity characterization of the thin film is described in the following section.

6.5. Property Characterization of Piezocomposites

Measurement procedures to determine matrix conductivity, electromechanical and dielectric property of piezocomposites and thin film resistance are described in sections below. Measurement results and discussion are detailed in the following chapter.

6.5.1. Matrix Conductivity Measurement

Initially, the four-point resistivity measurement method was used to estimate matrix conductivity. This is a DC technique where a voltage is applied across the sample and the resultant current is measured. Parallelepiped-shaped samples of conductive matrix at filler volume fractions ranging from 13.78% to 15% were prepared and electroded using air-dried silver. The DC technique was used with a Keithley 237 source measuring unit. However, it was noted that the current did not stabilize over long periods of time during the measurement. This is due to the inherent capacitance and the resistance of the conductive matrix creating an RC circuit type behavior.

To overcome this problem, an AC technique was used, where an LCR meter was used to measure the admittance of the conductive matrix sample at a desired frequency. A HP Model 4274 LCR meter was used for this purpose. The LCR meter directly outputs the values of the resistance and capacitance of the sample for an applied 1.0 Vrms over a frequency range of 100 Hz to 10 KHz.

6.5.2. d_{33} Measurement

For the thin film case, the piezocomposite samples were used to estimate d_{33} values before the thin film was deposited. This measurement was necessary to obtain an idea of the level of

poling in the fibers and to compare values for the continuous poling technique with the standard poling technique.

A Berlincourt piezo d_{33} meter was used for this purpose. The sample was lightly clamped between the two holders of the meter and excited at the desired frequency (100 Hz). The measured d_{33} value is displayed by the meter in 10^{-12} m/V. The d_{33} meter was designed to measure d_{33} for bulk piezoelectric samples and proved to be inaccurate for measuring d_{33} of these samples. A detailed discussion of this problem is in the next chapter.

6.5.3. Dielectric Constant Measurement

The dielectric constant of the piezocomposite in the thin film case was determined by measuring the capacitance of the sample across its electrodes. Though the PZT whiskers have high capacitance and the volume fraction of the whiskers was fairly high, the capacitance of the sample is very small (~ pF) because of its geometry (A << d). Because of this, an accurate low noise measurement setup (Figure 29) was developed based on a SR 850 DSP lock-in amplifier.

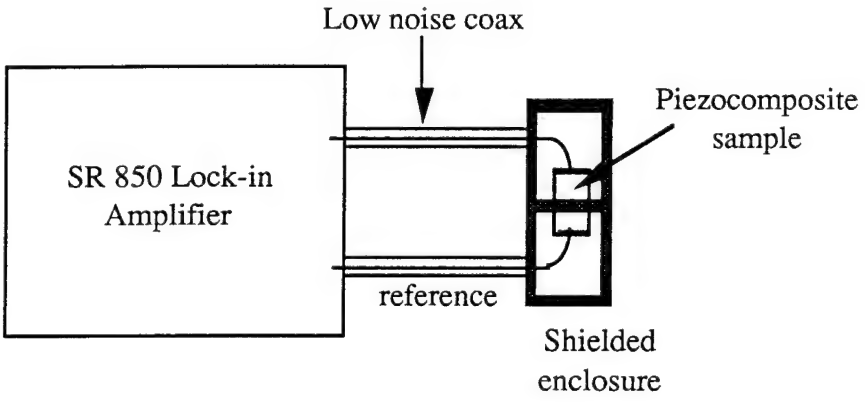

Figure 29. Schematic of Capacitance Measurement Setup

The setup consisted of the lock-in amplifier, low noise coax cables and a shielded enclosure to reduce stray capacitances. The lock-in provided a reference source signal at a desired voltage and frequency and measured the current across the sample. The SR 850 lock-in was capable of measuring currents in the fA (10^{-15}) range at the reference frequency. The lock-in displayed the magnitude of the measured current and the phase difference with respect to the reference voltage. Using standard impedance relations, the capacitance of the sample was calculated from the voltage and current. Impedance measurements were performed over a frequency range of 10 Hz - 1 KHz.

6.5.4. Thin Film Resistance Characterization

The setup for this measurement was the same as that for the capacitance measurement, except that the thin film sample was placed in the shielded enclosure instead of the piezocomposite sample. The lock-in measured the current across the film resistor for an applied voltage. The difference from the capacitance measurement was the phase difference between the reference voltage and measure current. For the resistor, the phase difference was 0°, as expected.

6.6. Dynamic Testing of Passively Damped Structure

There are two broad categories of frequency and damping measurement techniques for composite materials: resonant and sub-resonant methods. Resonant techniques are used when it is possible to excite resonance at a desired frequency in a specimen and are typically used for flexure and torsional vibration measurements. Sub-resonant techniques find applications in axial vibration measurements where, the resonant frequencies can be very high and hard to excite. This technique involves measuring the phase difference between the applied force and the displacement response for harmonic vibration. The main drawback with sub-resonant technique is the small phase angles that have to be measured, and it requires instrumentation with a high degree of precision.

For the beam-type specimen in consideration, a resonant flexural test is the simplest and a high degree of accuracy can be obtained. There are two resonant techniques that can be used: the first involves curve-fitting the frequency-response data in a narrow band around the resonance frequency to determine the frequency and damping, the second uses the free-decay technique at the resonant frequency to determine the frequency and damping. The first technique was used in this work.

Resonant techniques use frequency response data of the specimen. Frequency response of a specimen (also called the transfer function) can be determined from the ratio of the Fourier transforms of the excitation and response signals. A typical transfer function shows several resonant peaks and a resonant peak can be analyzed more accurately by performing a narrow band sweep. The excitation signal can be a random signal, an impulse type signal or a sine sweep type signal. Using a FFT analyzer, either of these excitation signals can be generated for testing.

A schematic of the test setup for a flexural resonant technique is shown below in Figure 30. The system analyzer generates the required excitation signal, which is applied to the specimen using a transducer. A power amplifier maybe used to amplify the excitation signal if necessary. A second transducer measures the beam response to the excitation and the system analyzer performs the FFT and calculates the transfer function for the system. Transducer placement is important and incorrect placement of the transducer can result in weak signals or missing a resonance peak. For a

cantilever beam type setup, the best locations for the transducers are at the root (for excitation) and at the tip of the beam (for response).

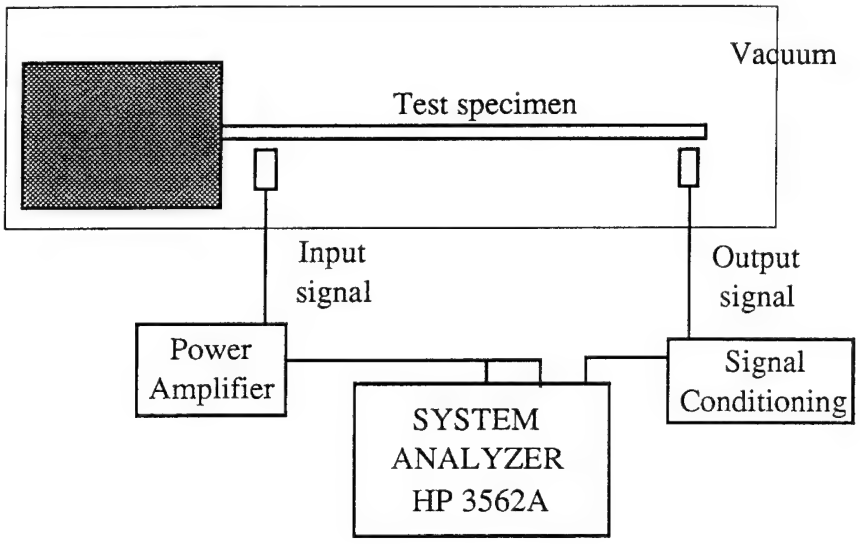

Figure 30. Schematic of Flexural Vibration Test Setup

A simple cantilever setup can be used to perform the test. For accurate measurements of the damping in the beam, the test setup should be placed in vacuum. The test procedure is fairly simple. An initial frequency response measurement will be performed over a wide frequency range to determine the first 5-6 resonant frequencies of the beam. A narrow band frequency response measurement will be performed at each of the first 5 frequencies and a curve fitting procedure will be performed to determine the frequency and damping at each resonant frequency. These measurements will be compared to the frequency and damping measurements for a baseline specimen, in order to estimate the damping increases.

If no damping increase is seen at the "design frequency" for the conductive matrix case, then the resonant frequency of the specimen will be altered by either adding small masses or changing the dimensions of the beam, and new frequency and damping measurements performed. In the thin film case, external shunt resistors will be used to study variation of damping with shunt resistance and the shunt resistance for peak damping determined. The corresponding film dimension will then be calculated to match the optimal shunt resistance and the film deposited on the piezocomposite sample. The dynamic tests will then be repeated to check the damping increases.

7. RESULTS AND DISCUSSION

7.1 Whisker/Conductive Matrix Composite

In this section, theoretical predictions and measurements for whisker/conductive matrix composites are presented. Theoretical predictions of second mode damping variation with matrix conductivity and beam geometry are presented. Also, the effect of two conduction paths is shown. Measurements of matrix conductivity and matrix elastic properties are shown along with corresponding theoretical predictions. Constituent properties are .

7.1.1 Theoretical Model Predictions

Based on the finite element based theoretical model presented, structural damping of a composite beam was predicted as a function of several paramaters. The beam basic configuration is similar to that outlined in Sec. 5.2, and is summarzied below.

The composite structure is a 2-layer piezocomposite beam, consisting of a base aluminum layer and a piezocomposite layer. The beam width and length is dictated by the availablilty of poled piezoelectric whiskers and are 1.0 cm and 8.1 cm respectively. A piezoelectric volume fraction of 20% is assumed for the piezocomposite layer. The matrix conductivity, aluminum beam thickness and piezocomposite layer thickness are design variables. The following sections show structural damping variations with design paramaters.

Structural damping variation with matrix conductivity

For the above beam configuration, Fig. 31 shows variation of beam modal damping (modes 1 to 4) as a function of matrix conductivity.

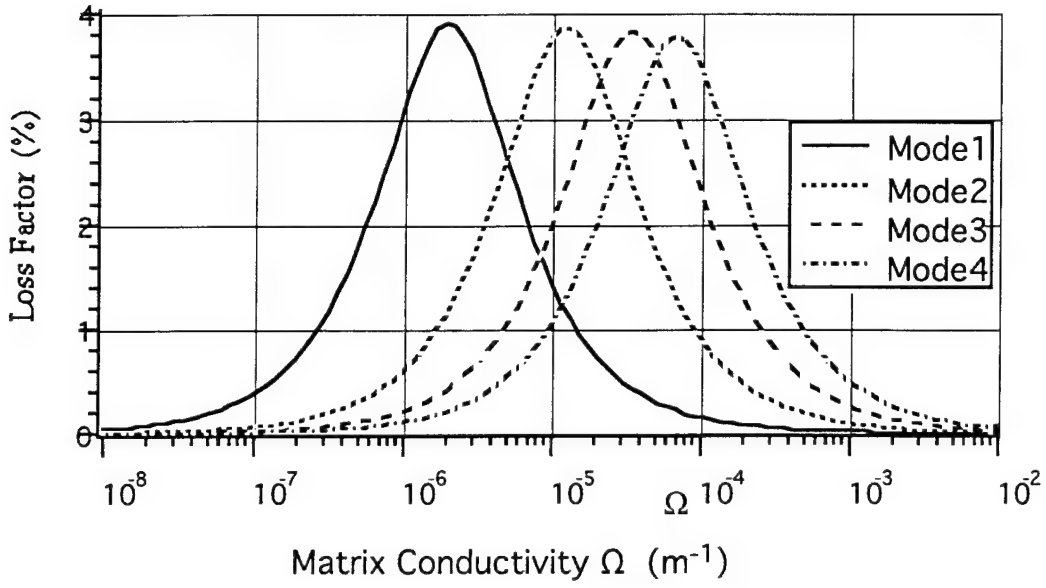

Figure 31 Variation of Modal Loss with Matrix Conductivity

The maximum loss is achieved in the first mode of approximately 4%. As expected, the ideal matrix conductivity is different for different modes and decreases with higher modes. The results shown in Fig. 31 are for the case where the resistive path is from end of one whisker to the end of the same whisker. The effect of the second resistive path (end of one whisker to end of adjacent whisker) is shown in Fig. 32.

The effect of a second resistive path is clearly seen in the first mode loss factor variation by the presence of a second peak. The effect of the second path is much smaller in the other modes and can be seen by the decrease in peak loss. For the first mode, the "bandwidth" of the peak loss variation is higher due to the second resistive path and is an advantage from a manufacturing point of view. However, the presence of a second path is generally detrimental to the overall performance of the structure.

It should be pointed out that the model only considers two possible resistive paths and based on the piezocomposite geometry being used, this is reasonable. Using different whisker arrangements and geometry can result in more than two resistive paths which can significantly alter the performance of the piezocomposite.

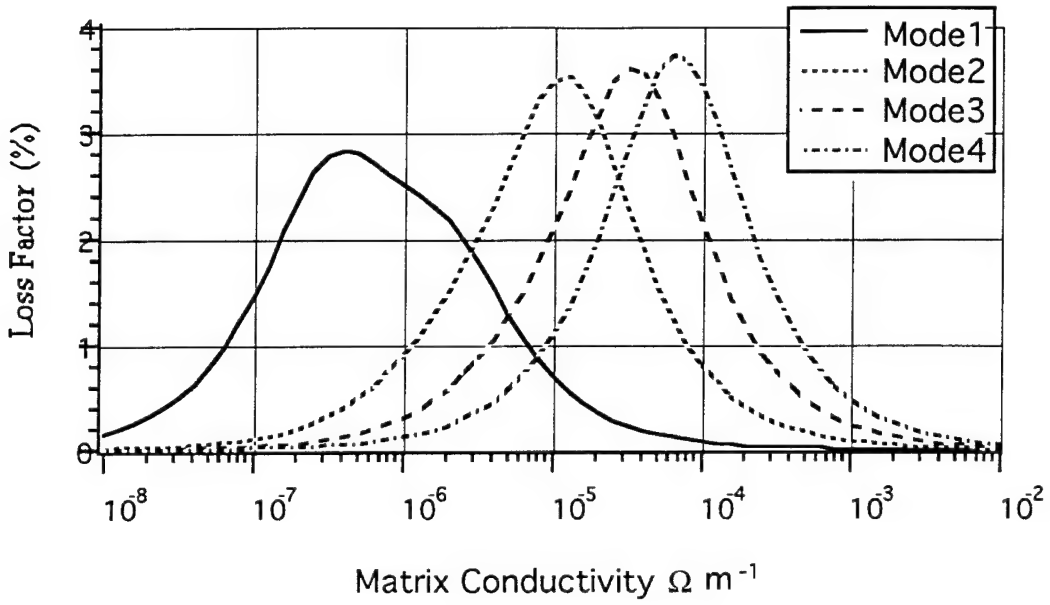

Figure 32. Modal Loss Factor Variation for Two Resistive Path Model

Structural damping variation with beam thicknesses

The next design variable considered was the aluminum beam thickness, keeping the piezocomposite layer thickness constant. The expected effect is an increase in modal loss factors in all the modes, upto a critical thickness followed by a decrease in modal loss. The initial increase is because of the increase in bending strain in the piezocomposite layer. The decrease after the critical thickness is due to the decrease in "effective" piezoelectric volume fraction in the structure. The critical thickness is where these two opposing effects balance out.

Figures 31 and 32 show modal loss factor variation with base beam thickness for two different matrix conductivities. In Fig. 31, the chosen matrix conductivity is for maximum loss in mode 1 and in Fig. 32 the conductivity corresponds to maximum loss in mode 2.

A comparison of Fig. 31 and 32 also shows the effect of choosing a particular matrix conductivity. Fig. 32 shows maximum loss factor in mode 1, but small loss factors for the other 3 modes, where as in Fig. 32, the maximum loss is in mode 2 and the other 3 modes show reasonable loss factors. Thus, choosing the correct matrix conductivity is dictated by the performance requirements of the structure.

In both cases (figs. 33 and 34), the ideal base beam thickness is the same (200 μm), which is equal to the piezocomposite layer thickness. This implies that the ideal base beam thickness is

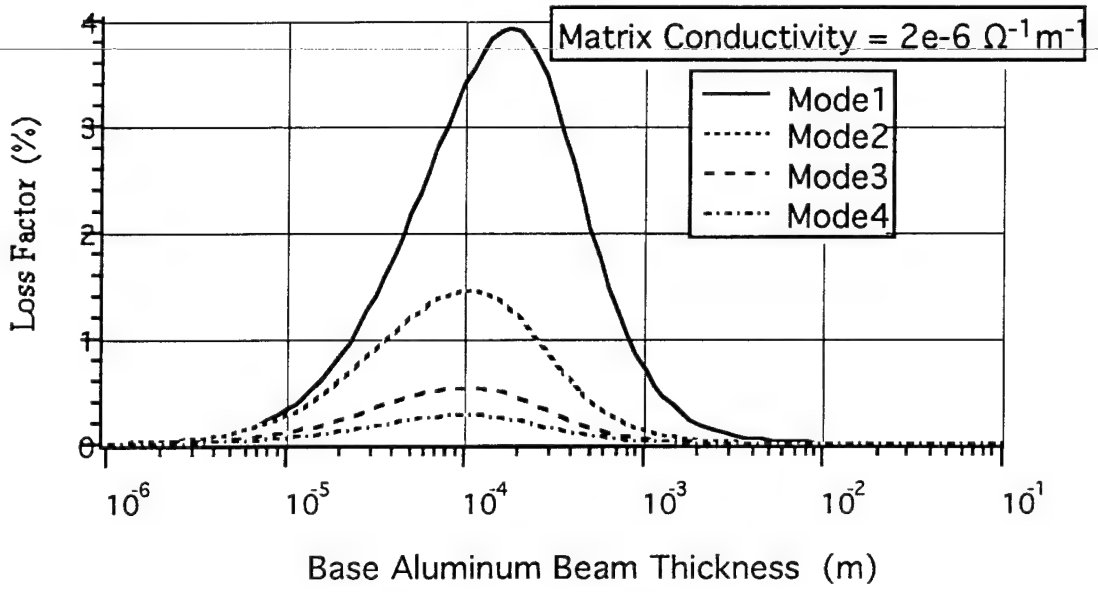

Figure 33. Modal Loss Factor Variation with Base Beam Thickness (case 1).

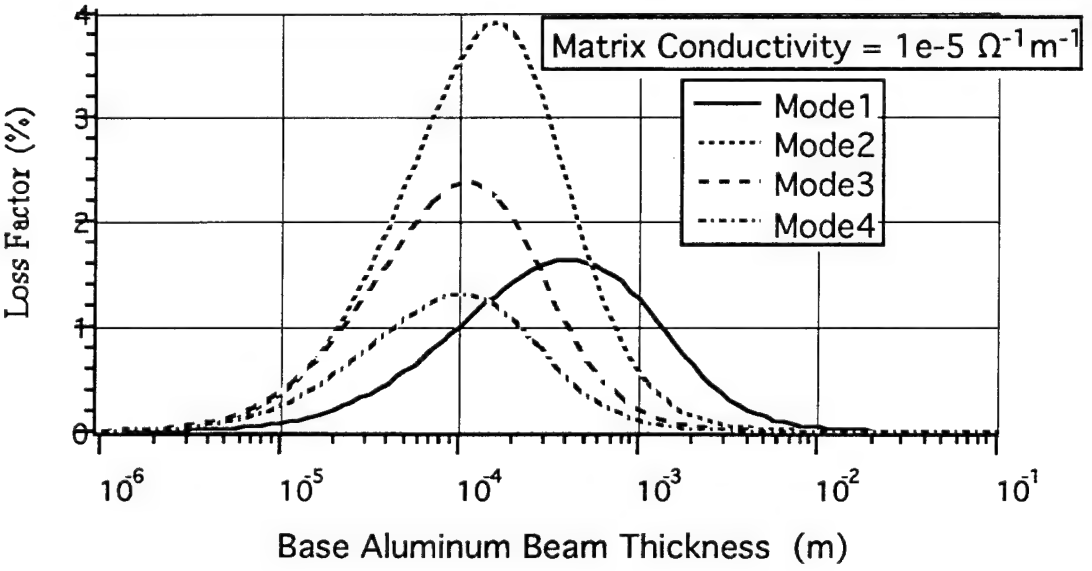

Figure 34. Modal Loss Factor Variation with Base Beam Thickness (case 2)

independant of the mode. While, the ideal base thickness is the same as the piezocomposite layer thickness in this configuration, in general they will not be the same. Increasing the "effective" piezoelectric volume fraction of the structure or using a different base beam material will alter the ideal base thickness.

Secondary design parameters

Other critical design parameters are "effective" piezoelectric volume fraction within the composite structure, piezoelectric properties of both the piezoceramic and the piezocomposite and structural geometry or configuration. Increasing "effective" piezoelectric volume fraction in the structure will cause a corresponding increase in the structural modal loss factors as well as structural stiffnesses. For all the predictions, a piezocomposite whisker volume fraction of 20% was used. The "effective" piezoelectric volume fraction for this case is dependant on the base beam thickness and for the case of equal piezocomposite layer and base beam thicknesses, the "effective" volume fraction is 10%. This is a fairly low number, and increasing it to >25% can yield significant increases in structural damping.

Increasing piezoelectric volume fraction increases structural loss by increasing the effective piezoelectric properties of the composite. For the current study, PZT-5H was chosen as the piezoceramic material. The main advantage of using PZT-5H was the ease of poling the material. However, it had a low Curie temperature (193 °C), which placed some restrictions on the manufacturing process (cure temperatures). Other materials should be studied, based on the performance requirements of the composite, particularly the Curie temperature.

The present study was performed only for the composite beam configuration outlined in Sec. 5.2. A beam configuration was chosen because of the simplicity of performing dynamic tests on beams. Many other configurations are possible and can have significantly different behavior from that predicted in this study.

7.1.2 Experimental Results

Initial work focused on controlling the matrix conductivity as a function of the conductive filler volume fraction. Dimensions of conduvtive matrix samples for resistivity measurements are shown in Table 7.1.

Table 7.1 Filler/Epoxy Sample Data

	Distance between electrodes (mils)	Width (mm)	Height (mm)	d/A (1/m)	A/d (m)
Pure Epoxy	1	9	6.5	0.2303	4.342
15% filler	65	13.8	49.5	24.155	0.0414
14.75% filler	36	11.67	5.21	15.048	0.0665
14.5% filler	47	9.36	5.16	24.736	0.0404
13.77% filler	42.5	15.3	48.3	14.62	0.0684

Following the procedure outlined in Sec. 6.5, the resistance and capacitance of the four samples were measured. As mentioned before, a dc resistance measurement is not possible because of the capacitive effect of the conductive matrix. The volume fractions chosen for characterization were based on earlier work[14] on the same filler/epoxy system. During manufacture, it was fairly easy to control the filler volume fraction accurately to within 0.05%. Table 7.2 shows the measured resistivities and dielectric constants of the samples.

As expected, the resistivity of the conductive matrix system decreases with increase in filler volume fraction. The percolation effect is also seen by the large drop in resistivity of the material for a small increase in volume fraction.

Table 7.2 Dielectric Constant and Resistivity for Filler/Epoxy Samples

	Pure Epoxy	15% filler	14.75% filler	14.5% filler	13.77% filler
Dielectric Constant 100Hz 1 KHz 10 KHz	1.47	3900 2760 1965	2345 1895 1166	2413 2037 1286	1.98
Resistivity 100Hz 1 KHz 10 KHz (ohm.m)	-	9.133e2 9.025e2 7.038e2	1.616e3 1.573e3 1.136e3	2.731e3 2.602e3 1.426e3	4.15e5

The side effect of the percolation effect was the increase in dielectric constant. There has been little work in the literature on characterization of dielectric properties of filler/epoxy systems in the region of the percolation effect. This behavior of the system, was unforseen and posed a significant problem. The large change in dielectric property of the conductive matrix, alters the RC behavior (outlined in chapter 5) significantly. The matrix conductivity was predicted by the theoretical model based on constant dielectric property for the filler/matrix system. Obviously as seen from Table 7.2, this is not the case. Thus, both the dielectric as well as the resistive behavior have to be included in the model, which complicates the procedure considerably. This was the main reason for switching to the whisker/thin film configuration for further study.

7.2 Whisker/Thin Film Piezocomposite

For the beam structural geometry outlined in Sec. 5.4.2, theoretical predictions of structural loss factor are presented for variations in the design parameters. In all cases, the thin film was assumed to have a constant thickness of 1 μm, and the film resistivity/conductivity was assumed to be variable. Experimental results are presented for property characterization of thin films and piezocomposite specimens.

7.2.1 Theoretical Predictions

Predictions of beam modal loss factor are presented in the following sections as functions of various design parameters. The critical design paramaters are thin film conductivity/resistivity, base beam geometry, "effective" piezoelectric volume fraction in the beam and location of piezocomposite specimens on the base beam. In all the cases, unless mentioned specifically, the structural dimensions are those outlined in Sec. 5.4.2. Two specific cases are compared: case 1 where there are two piezocomposite specimens bonded near the root on the same side of the base beam, and case 2, where there are piezocomposite specimens bonded along the entire length of the beam.

Structural loss factor variation with film conductivity

Fig. 35 (a) and (b) show the modal loss factor variation with film conductivity for the beam configurations (cases 1 and 2). It is interesting to note that, for case 1, the peak loss for mode 1 is highest of the four modes and mode 3 has smaller peak loss than mode 4. This is due to the geometry and configuration of the beam. Note that in this case, there are only two piezocomposite specimens adjacent to each other at the root of the base beam and on the same side. One can expect the results to be different if there are specimens placed along the entire length of the beam (case 2), and the results for this case are shown in Fig. 35(b).

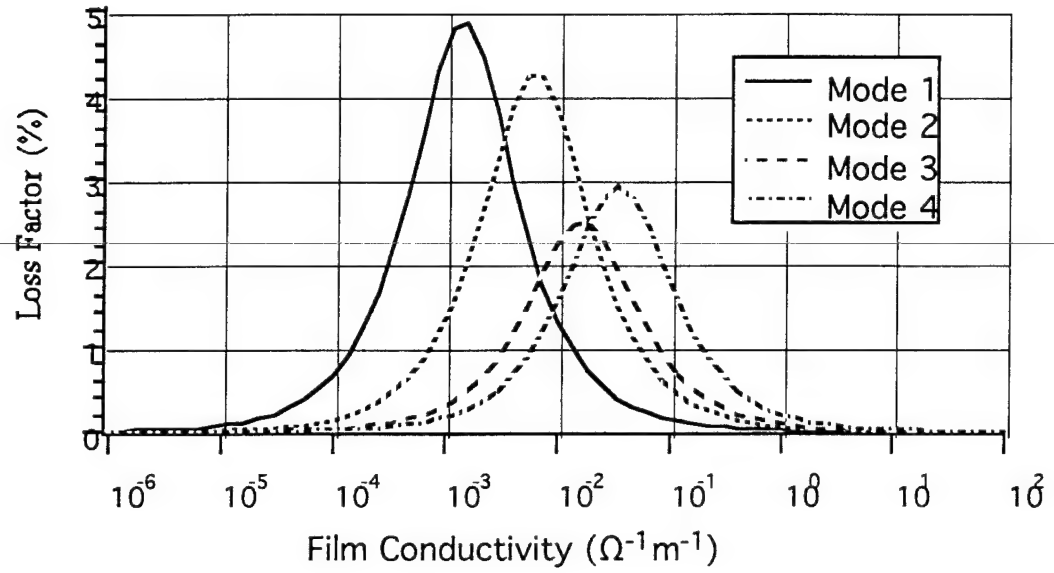

Figure 35(a). Modal Loss Factor Variation with Thin Film Conductivity (case 1).

Case 1

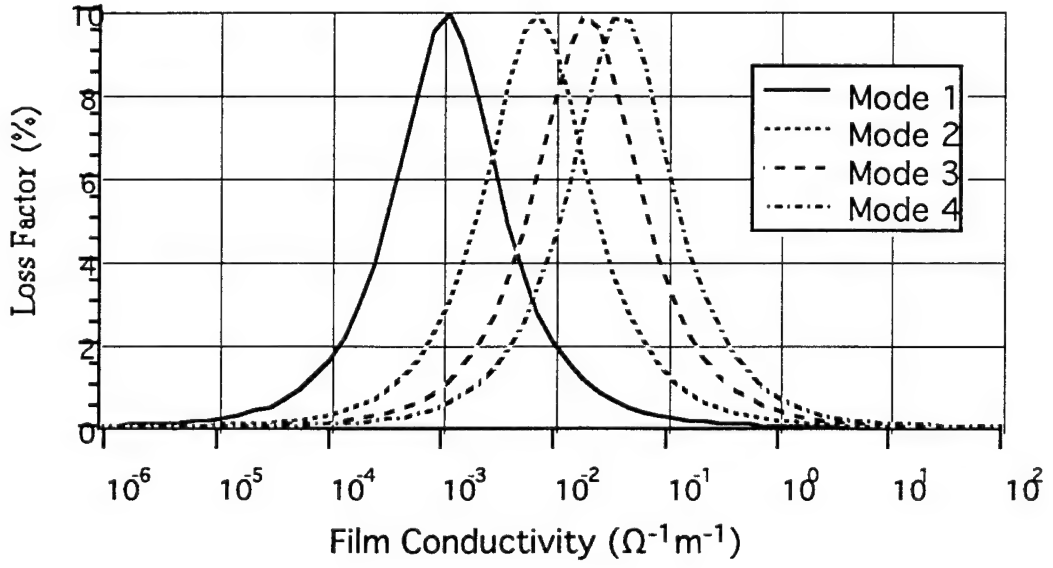

Figure 35(b). Modal Loss Factor Variation with Thin Film Conductivity (case 2).

Case 2

In case 1, where there are only 2 piezocomposite specimens bonded to the base beam, the location of the two specimens along the length plays a critical role in the modal loss. Location of the specimen at a node of a particular mode, will reduce the damping performance of the structure in that mode, which is the case in mode 3 in Fig. 35(a). When there are specimens along the entire length, it is no longer critical. Also, the loss factors in case 2 are much higher than case 1, because the "effective" piezoelectric volume fraction is much higher.

Comparing the results in Figs. 35 (a) and (b) with those in Figs. 31 and 32 (the whisker/conductive matrix composites), it is obvious that modal loss factors are much higher. The main reason for this is the increase in piezoelectric volume fraction. It was much easier to manufacture high volume fraction (40%) piezocomposite specimens, compared to the conductive matrix piezocomposite layer. The presence of the filler in the matrix increased viscosity and hardness of the matrix. As a result, it was harder to pack a large number of fibers within the same amount of matrix and also harder to grind the piezocomposite layer after cure (to reduce thickness). The main disadvantage with thin film piezocomposites is that the final product is a rectangular specimen and many of them have to be bonded onto the structure, where as in the conductive matrix case, the final product was a single piezocomposite layer which could be easily incorporated into the structure.

Structural loss factor variation with base beam thickness

Base beam thickness is a critical parameter because in flexural vibration, the strain in the piezocomposite specimen is a function of the base beam thickness. Increasing base beam thickness increases the strain and accordingly the modal loss factor, but increasing base beam thickness also decreases the "effective" piezoelectric volume fraction of the structure. Fig. 36 (a) (case 1) and Fig. 36 (b) (case 2) show the effect of base beam thickness variation on modal loss factors.

There is a significant difference in the behavior at higher modes between cases 1 and 2 and the reason for this is the location of the piezocomposite specimens and the length of the specimen as compared to the beam length.

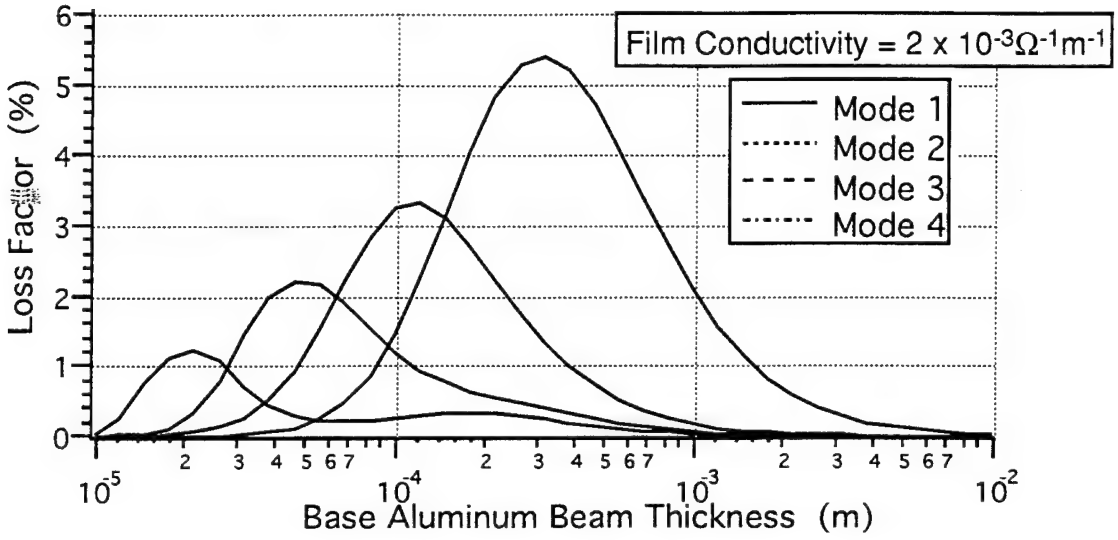

Figure 36 (a). Loss Factor Variation with Base Beam Thickness (case 1)

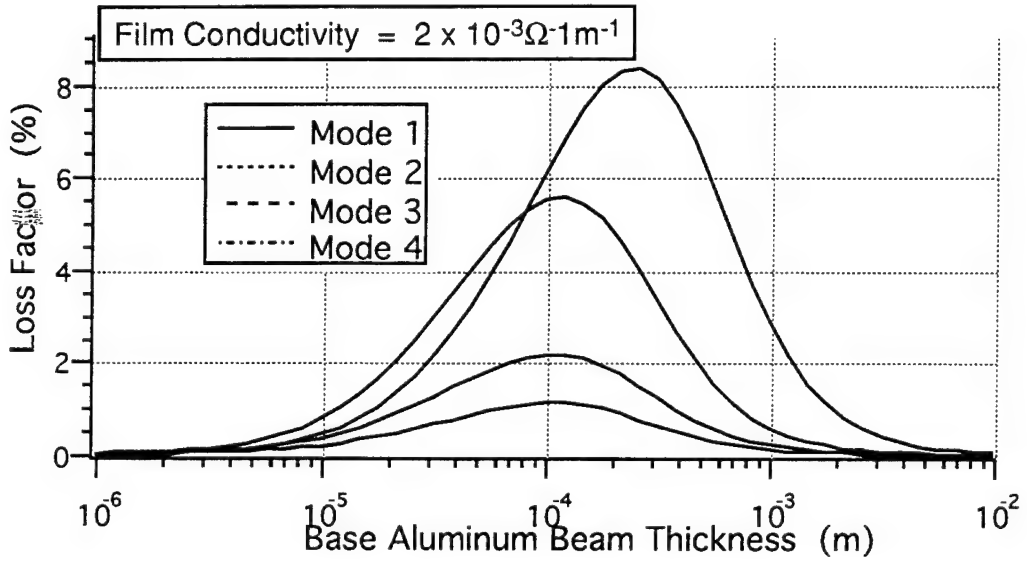

Figure 36 (b). Loss Factor Variation with Base Beam Thickness (case 2)

In the configuration modeled, the beam length is 6 times the piezocomposite specimen length. For higher modes (3 and higher), the length of the specimen becomes significant, because of the mode shapes and the location of nodes. If a specimen is located at or near a node, the effective strain between the ends (electrodes) of the specimen is close to zero and there is no damping. Increasing the beam length will solve the problem, however, increasing beam length

also changes the piezoelectric volume fraction. In order to maintain the same volume fraction, more specimens (more poled fibers) are required.

Secondary design parameters

Using thin film piezocomposites adds an extra design parameter compared to the conductive matrix case. Since the piezocomposite specimen is small and can be located at different positions on the structure (beam), the location of the specimen can be chosen to be a region of high strain energy for the particular mode. This concept has already been demonstrated[17,19] by using externally shunted piezocomposites for damping a cantilever beam.

A significant advantage of using thin film piezocomposites is that there is only one resistive path in the composite (the thin film). This simplifies the modeling approach considerably and also does not place any restrictions on the piezocomposite geometry or whisker packing geometry, as was the case for the conductive matrix composite.

7.2.2 Experimental Results

Each piezocomposite specimen was characterized for its properties after manufacture. Table 6.3 lists the specimen properties and dimensions. The specimen numbers are in chronological order and show the "learning curve" effect regarding specimen piezoelectric whisker volume fraction. Compared to conductive matrix specimens, these specimens were relatively easier to manufacture and higher volume fractions were obtained.

Piezoelectric properties

The d_{33} values shown in the Table are approximate, because of the specimen geometry. The specimen is very thin (8 mils or 200 μm), which made it extremely difficult to measure the d_{33} using a standard d_{33} meter. The problem is with the electrodes on the d_{33} meter, which were designed for bulk samples. The meter is designed to measure uniform strain across a bulk sample for an applied voltage at a known frequency, and the electrodes are point contact electrodes. Because of the thin wafer like geometry, point contact electrodes cannot be used, as the measured strain at that point is not the same as the "uniform strain" across the specimen. Also, the specimens buckle very easily (due to the geometry), and care must be taken when holding the specimen between the electrodes. Erroneous values can be measured for a buckled specimen as the buckled specimen will show large values of strain for a small load. For these reasons, the d_{33} values shown in Table are approximate. The value in brackets is the measured value for reversed polarity.

Table 7.3 Piezocomposite Specimen Data

Specimen Number	Length (mm)	Width (mm)	Thickness (mils)	Number of fiber segments	Volume fraction of PZT	d_{33} (10^{-12} strain/(V/m))
1	11	7	8	40	31.8%	142 (-147)
2	11	7	8	44	35%	78 (-91)
3	11	7	7.5-8	44	35%	181 (-180)
4	11	7	8	43	34.2%	130 (-126)
5	11	6	8	43	39.8%	280 (-260)
6	11	6	7	45	47.7%	290 (-301)
7	11	6	7.5	44	43.5%	271 (-275)

Note: d_{33} measurements are approximate, due to specimen geometry.

Dielectric properties

Dielectric properties of the piezocomposite specimens were measured as detailed in Chapter 6. Figure 37 shows a typical measurement for a specimen. An impedance measurement was performed for each specimen over a frequency range and the Fig. 38 shows magnitude of the measured current as a function of the frequency. The measured phase angle for all the specimens was always greater than 80° over the frequency range of interest, which shows that the resistivity is extremely high and the conductivity can be assumed to be zero for practical purposes (one of the assumptions in modeling).

The straight line fit, along with standard parallel RC circuit equations, is used to derive the value of the capacitance of the specimen and the dielectric constant is calculated from the specimen geometry.

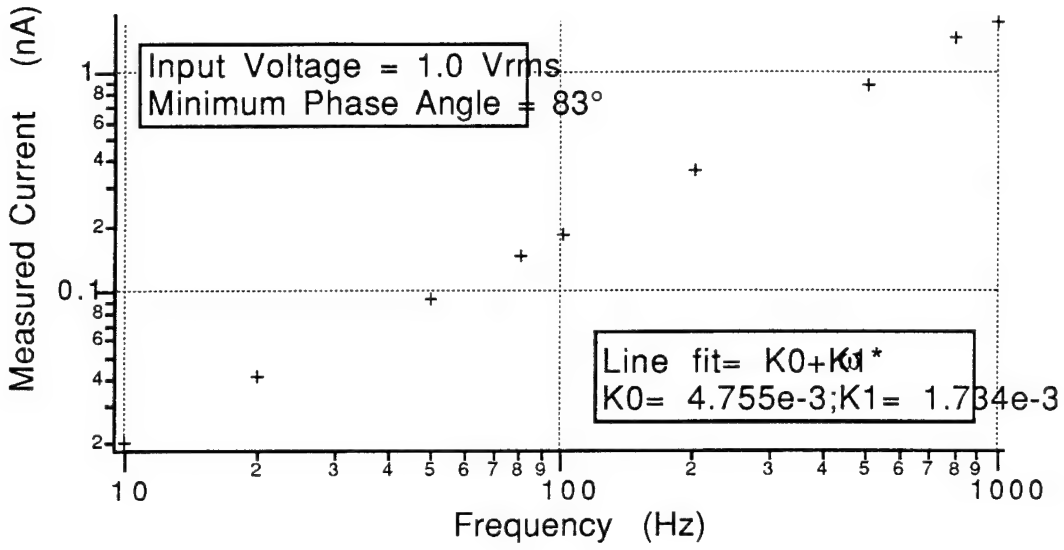

Figure 37 Typical Electrical Response of a Piezocomposite Specimen

Table 7.4 shows the measured capacitance and dielectric constant values for each of the specimens. Several facts stand out from this Table. The small A/d shows that the geometry of the specimen plays a big role in determining the effective capacitance of the specimen. The capacitance of the specimen is important because it directly affects the electrical time constant of the shunted piezoelectric. The measured capacitance values are also very small. This posed several problems in the measurement stage. A special shielded box was built for this purpose to reduce any stray capacitances. Low noise coax cables were also used and a high resolution lock-in amplifier was necessary because of the very small currents being measured.

Because of the small capacitances of each piezocomposite specimen, the required shunt resistance for peak damping in the 100 - 1 KHz range is very high. Estimated values of shunt resistance are in the 100 - 1000 Mohm range. For the thin film case shown in Fig.35, for first mode peak damping, the corresponding shunt resistance is 917 Mohm.

Table 6.4 Capacitance and Dielectric Constant Data

Specimen Number	Capacitance (pF)	A/d (μm)	Dielectric Constant
1	1.73	129.31	1511
2	0.93	129.31	812
3	0.93	125.27	838
4	1.75	129.31	1528
5	5.46	110.84	5564
6	4.15	96.98	4833
7	4.27	103.91	4641

Thin film characterization

Thin films were characterized by the procedure described in Sec. 5.5. Four different films were deposited on an epoxy substrate and an impedance measurements were performed for an applied voltage of 5V. The results are shown below in Table 6.5.

Table 7.5 Measured Resistivities for Thin Films

Film Number	Thickness (Angstrom)	Current (pA)	Resistivity (ohm.m)
1	1665	11.2	1.062e4
2	1511	13.05	8.27e4
3	1500	10.6	1.011e5
4	1260	12.47	7.217e4

The measured resistivity was slightly higher than that required range (10^1 - 10^4 ohm.m). The film thicknesses, were an order of magnitude smaller than the design thickness of 1 micron. The required resistivity range can be obtained by depositing thicker films (~ 1 micron).

7.3. Composite Beam Dynamic Testing

Dynamic tests to determine modal frequencies and loss factors of a composite beam with whisker/thin film piezocomposites are currently being done. Results of these tests will be published at a later date.

8. CONCLUSIONS

Fine scale lead zirconate titanate (PZT), niobium substituted PZT (Nb-PZT), lanthanum substituted PZT (PLZT) piezoelectric fibers were fabricated from sol-gel processed viscous "sol" using the spinning methodology developed for the continuous glass/carbon fibers. For the fiber fabrication process, studies on the two areas were emphasized: formation of stable "sol" and dense fiber by studying sol-gel chemistry and sintering temperatures. PZT fiber diameter of 20–60 μm were successfully produced with sintering temperature above 700°C. The higher temperature was required to further increase density of the fiber, which was associated with grain growth.

Also, the characterization methods of such fine ferroelectric fibers were studied. The dielectric constant and polarization hysteresis of single fibers were measured showing similar characteristics as bulk (disk) samples. Continuous PZT fiber data on tensile strength was also produced on single fibers showing the range of 30 to 55 MPa.

The use of PZT fiber for shunted composite applications was also studied extensively using both analytical and Finite Element Modeling method. The experiment was performed using CeraNova extruded PZT-5H fiber (diameter: 120 μm) for the ease of handling. Due to the difficulty arising from the use of axially poled continuous fiber, PZT whiskers with high aspect ratio (100) was used for composite study. Though ideal shunt piezo composite contains PZT whiskers with controlled resistivity coating which is a feasible technology, we have tried mixing polymer matrix with conductive particles first. The following problems surfaced: (1) percolation theory makes it difficult to control precise resistance of the polymer-conductor particle mixture, (2) high viscosity of matrix during the mixing makes high PZT fiber loading difficult, (3) common matrix creates multiple conduction paths among the whiskers, which makes modeling task nearly impossible, (4) increase in conductive phase in matrix also increased effective dielectric constant of the matrix, which again makes modeling task difficult. Therefore, the surface resistive coating of piezo composite made with PZT whiskers in insulating epoxy matrix was performed.

Both theory and experiment results were presented in this report.

REFERENCES

1. S.K. Kurtz and S. Yoshikawa, Annual Technical Report to ONR, "Passive Damping," Grant No. N00014-90-J-1540, Jan. 1991.

2. S.K. Kurtz and S. Yoshikawa, Final Technical Report to ONR, "Passive Damping Materials: Piezoelectric Ceramic Composites for Vibration Damping Application," Grant No. N00014-J90-1540, June 1992.

3. K. Kamiya, H. Honda, and H. Nasu, "Sol-gel Processing of $PbTiO_3$ Ceramic Fibers," Jpn. J. Ceram. Soc. 98, 759–64, 1990.

4. U. Selvaraj, A.V. Prasadarao, S. Komarneni, K. Brooks, and S. Kurtz, "Sol-gel Processing of $PbTiO_3$ and $Pb(Zr_{0.52}Ti_{0.48})O_3$," J. Mater. Res. 7, 992–6 (1992).

5. K.D. Budd, S.K. Dey, D.A. Payne, Brit. Ceram. Proc. 39, 107 (1985).

6. S. Yoshikawa, U. Selvaraj, P. Moses, J. Witham, R. Meyer, and T. Shrout, "$Pb(Zr,Ti)O_3$ (PZT) Fibers—Fabrication and Measurement Methods," Journal of Intelligent Material Systems and Structures, Vol. 6, No. 3, 152–158 (1995).

7. T.R. Gururaja, D. Christopher, R.E. Newnham, and W.A. Schulze, "Continuous Poling of PZT Fibers and Ribbons and Its Application to New Devices," Ferroelectrics, 47, 193–200, 1983.

8. Q.C. Xu and Q. Jiang, "A Poling Technique for Piezoelectric Fibers and Fiber Property Characterization," Ferroelectrics, Vol. 156, pp. 85–90 (1994).

9. A. von Hipple, Dielectrics and Waves, 1954, New York: Wiley, p. 240.

10. S. Yoshikawa, U. Selvaraj, P. Moses, Q. Jiang, and T. Shrout, "$Pb(Zr,Ti)O_3$ (PZT) Fibers—Fabrication and Properties," Ferroelectrics, Vol. 154, 324–330 (1994).

11. Hagood, N.W., Hall S. and Crawley, E., "Smart Structures for Rotorcraft Consortium Kickoff Meeting: MIT Background Programs," Jan. 1994.

12. Cox, H.L., "The Elasticity and Strength of Paper and Other Fibrous Materials," British Journal of Applied Physics, Vol. 3, March 1952, p. 72.

13. Yoshikawa, S., Ota, T. and Newnham, R.E., "Piezoresistivity in Polymer-Ceramic Composites," Journal of American Ceramic Society, Vol. 73, No. 2, 1990, pp 263-267.

14. Ruschau, G.R., Yoshikawa, S. and Newnham, R.E., "Resistivities of Conductive Composites," Journal of Applied Physics, Aug. 1992.

15. Ruschau, G.R., Yoshikawa, S. and Newnham, R.E., "Conductor-Polymer Composite for Electronic Connectors," Ceramic Transactions: Advanced Composite Materials, Vol. 19, American Ceramic Society, Westerville, Ohio, 1991

16. Lesieutre, G.A., Yarlagadda, S., Yoshikawa, S., Kurtz, S.K. and Xu, Q.C., "Passively Damped Structural Composite Materials Using Resistively Shunted Piezoceramic Fibers," Journal of Materials Engineering and Performance, Vol. 2(6), Dec. 1993, pp. 887-892.

17. Hagood, N.W. and von Flotow A., "Damping of Structural Vibrations with Piezoelectric Materials and Passive Electrical Networks," Journal of Sound and Vibration, Vol. 146, No. 1, April, 1991.

18. Edberg, D., Bicos, A.S., Fuller, C.M., Tracy, J.J. and Fechter, J.S., "Theoretical and Experimental Studies of a Truss Incorporating Active Members," Journal of Intelligent Materials, Systems and Structures, Vol. 3, 1992, pp. 333-347.

19. Lesieutre, G.A. and Davis, C.L, "Frequency Shaped Passive Damping Using Resistively-Shunted Piezoelectrics," Proc. of Symposium on Active Materials and Adaptive Structures, Nov. 1991, pp. 355-358.

20. Chan, H.L. and Unsworth, J., "Simple Model for Piezoelectric Ceramic/Polymer 1-3 Composites Used in Ultrasonic Transducer Applications," IEEE Transactions on Ultrasonics, Ferroelectrics and Frequency Control, Vol. 36, 1989, pp. 434-441.

21. Cao, W., Zhang, Q. and Cross, L.E., "Theoretical Study on the Static Performance of Piezoelectric Ceramic Polymer Composites with 1-3 Connectivity," Journal of Applied Physics, Vol. 72, No. 12, 1992.

22. Sottos, N.R., Li, L, Scott, W.R. and Ryan, M.J., "Micromechanical Behavior of 1-3 Piezocomposites," SPIE, Vol. 1916, 1993, pp. 87-96.

23. Beneveniste, Y. and Dvorak, G.J., "Uniform Fields and Universal Relations in Piezoelectric Composites," Journal of Mechanics and Physics of Solids, Vol. 40, No. 6, 1992, pp. 1295-1312.

24. Dunn, M.L. and Taya, M., "Micromechanics Predictions of the Effective Electroelastic Moduli of Piezoelectric Composites," International Journal of Solids and Structures, Vol. 30, No. 2, 1993, pp. 161-175.

25. Dunn, M.L., "Exact Relations Between the Thermal and Electroelastic Moduli of Composite Materials with Emphasis on Two-Phase Laminates," SPIE, Vol. 1916, 1993, pp. 275-285.

26. Allik, H. and Hughes, T.J.R., "Finite Element Method for Piezoelectric Vibration," International Journal for Numerical Methods in Engineering, Vol. 2, 1970, pp. 151-157.

27. Tiersten, H.F., "Linear Piezoelectric Plate Vibration," Plenum Press, 1969.

28. Tzou, H.S. and Tseng, C.I., "Distributed Vibration Control and Identification of Coupled Elastic/Piezoelectric Systems: Finite Element Formulation and Applications," Mechanical Systems and Signal Processing, Vol. 5, No. 3, 1991, pp 215-231.

29. Ha, S.K., Keilers, C. and Chang, F.K., "Finite Element Analysis of Composite Structures Containing Distributed Piezoceramic Sensors and Actuators," AIAA Journal, Vol. 30, No. 3, 1992, pp 772-780.

30. Hladky-Hennion, A.C. and Decarpigny, J.N., "Finite Element Modeling of Periodic Structures: Application to 1-3 Piezocomposites," Journal of Acoustic Society of America, Vol. 94, No. 2, Pt. 1, Aug. 1993, pp 621-635.